



Optimal layout design of obstacles for panic evacuation using differential evolution



Yongxiang Zhao^{a,b}, Meifang Li^{a,*}, Xin Lu^c, Lijun Tian^a, Zhiyong Yu^d, Kai Huang^a, Yana Wang^a, Ting Li^a

^a School of Economics and Management, Fuzhou University, Fuzhou 350108, China

^b Department of Civil and Environmental Engineering, University of California, Davis, CA 95616, USA

^c College of Information System and Management, National University of Defense Technology, Changsha 410073, China

^d College of Mathematics and Computer Science, Fuzhou University, Fuzhou 350108, China

HIGHLIGHTS

- Differential evolution is used to optimize the geometrical parameters of obstacles.
- Profiles of density, velocity, specific flow as well as crowd pressure are analyzed.
- Placing an obstacle in panic situations promotes the pressure to a much higher level.
- Physical mechanism of efficiency enhancement is a reduction of high density region.
- Panel is more robust than pillar to guarantee the enhancement of pedestrian outflow.

ARTICLE INFO

Article history:

Received 13 April 2016

Received in revised form 5 July 2016

Available online 20 August 2016

Keywords:

Panic evacuation

Social force model

Obstacle optimization

Pedestrian outflow

Differential evolution

Crowd pressure

ABSTRACT

To improve the pedestrian outflow in panic situations by suitably placing an obstacle in front of the exit, it is vital to understand the physical mechanism behind the evacuation efficiency enhancement. In this paper, a robust differential evolution is firstly employed to optimize the geometrical parameters of different shaped obstacles in order to achieve an optimal evacuation efficiency. Moreover, it is found that all the geometrical parameters of obstacles could markedly influence the evacuation efficiency of pedestrians, and the best way for achieving an optimal pedestrian outflow is to slightly shift the obstacle from the center of the exit which is consistent with findings of extant literature. Most importantly, by analyzing the profiles of density, velocity and specific flow, as well as the spatial distribution of crowd pressure, we have proven that placing an obstacle in panic situations does not reduce or absorb the pressure in the region of exit, on the contrary, promotes the pressure to a much higher level, hence the physical mechanism behind the evacuation efficiency enhancement is not a pressure decrease in the region of exit, but a significant reduction of high density region by effective separation in space which finally causes the increasing of escape speed and evacuation outflow. Finally, it is clearly demonstrated that the panel-like obstacle is considerably more robust and stable than the pillar-like obstacle to guarantee the enhancement of evacuation efficiency under different initial pedestrian distributions, different initial crowd densities as well as different desired velocities.

© 2016 Elsevier B.V. All rights reserved.

* Corresponding author.

E-mail address: limeifang@fzu.edu.cn (M. Li).

1. Introduction

In recent years, pedestrian evacuation in case of emergencies, such as fire, earthquake, tsunamis, or a terrorist attack, has attracted considerable attention. Traffic behaviors have been successfully reproduced by statistical physics models including social force model [1–3], cellular automation models [4–6], lattice gas models [7–10] and queueing-based models [11] proposed by MacGregor Smith and Cruz [11]. These models provide important design guidelines for transportation and building environment [12–15], as well as offering strategies for emergency evacuation in all kinds of natural or man-made disasters [16–18].

In panic situations, where people push each other to get out of a room, it is possible to increase the outflow by suitably placing an obstacle in front of the exit [1,19–24]. Obstacles may enhance pedestrian flow by more than 30% and even double the flow that would occur without the obstacle [25]. However, the obstacle's size and placement should be properly tuned in order to obtain an optimal improvement in the evacuation time. When these geometrical parameters of obstacles are unsuitable, the area near the exit may become more crowded which will slow down the outflow rather than increase it. For instance, it will become harmful and inefficient for obstacles placed symmetrically near the exit door. Therefore, the best way for achieving an optimal evacuation outflow is to shift the obstacle slightly from the center of the exit [26,27].

Although a significant amount of researches have already been performed on how to control the pedestrian outflow and to maximize the escape velocity in panic situations, there is no very simple but effective approach to obtain the optimal geometrical parameters of obstacles, including the optimal size of obstacle, the optimal obstacle–door gap and asymmetric offset distance of obstacle to the center of the exit. Recently, genetic algorithm was used to provide the layout design of the obstacles that can reduce the tangential momentum and increase the escape speed [20]. However, in their works, only pillar-like obstacles were considered. In fact other shaped obstacle such as a thin flat panel also has ability to enhance the outflow efficiency. G.A. Frank et al. investigated the impact of human behavior on an escaping situation, obstructed by a pillar and a panel close to the door [19]. Although their papers showed clearly that both pillar and panel are simple and effective shapes of obstacle, they did not tell us what is the optimal layout for pillar-like obstacle and panel-like obstacle. Therefore, the main objective of our paper is to find an optimal tuning on obstacle size and placement in order to achieve a minimum leaving time for all the pedestrians in the room, and a differential evolution will be used to provide the optimal layout design of pillar-like and panel-like obstacles.

Moreover, Kirchner et al. proposed that placing an obstacle in panic situations might avoid clogging near the exit by absorbing pressure, and consequently, the clogging effects translate to an early stage [26]. Helbing et al. suggested that the obstacle may behave like a wave breaker to absorb the pressure in the crowd and to reduce it to a subcritical level [25]. Zuriguel et al. also agreed that the physical mechanism behind the clogging reduction while placing an obstacle is a pressure decrease in the region of arch formation [23]. However, to our knowledge, the spatial distribution of pedestrian pressures are rarely directly compared among the different shaped obstacles. Therefore, in this paper, we will further calculate the maximum pressure, the average pressure, and the spatial distribution of pedestrian pressures among no obstacle, pillar-like obstacle and panel-like obstacle in order to prove that placing an obstacle can reduce the pressure in the region of exit or, on the contrary, increase the pressure to a more dangerous level.

The paper is then organized as follows. Firstly, a robust differential evolution (DE) is employed to optimize the geometrical parameters of different shaped obstacles in order to achieve a minimum leaving time for all the pedestrians in the room. Then the effects of these geometrical parameters of obstacles on evacuation time have been further analyzed respectively, including the size of obstacle, the obstacle–door gap and the offset distance of obstacle to the center of the exit. Moreover, to uncover the essence of evacuation performance enhancement, the profiles of density, velocity and specific flow for no obstacle, pillar-like obstacle and panel-like obstacle are compared based on the Voronoi method, and the panel-like obstacle can significantly decrease the high crowd density near the area of exit which leads to the remarkable enhancement of escape speed and pedestrian outflow. Especially, the maximum pressure, average pressure, and the spatial distribution of pedestrian pressures among no obstacle, pillar-like obstacle and panel-like obstacle are analyzed, and it is clearly demonstrated that placing an obstacle surprisingly increases the average crowd pressures in the region of exit which is markedly different from the hypothesis of existing literature. Finally, to further verify the robustness and universality of evacuation performance for different shaped obstacles, we have compared the evacuation time among no obstacle, pillar-like obstacle and panel-like obstacle under different initial pedestrian distributions, different initial crowd density, and different desired velocities of escape.

2. DE-based geometrical parameters optimization of obstacles

2.1. Social force model

The social force model [1–3] is a pedestrian behavior model based on socio-psychological and physical forces. It assumes that each pedestrian meets the laws of motion as a particle, and uses force vectors to describe the real force and the intrinsic motivation. Each of N pedestrians i of mass M_i likes to move with a certain desired speed v_i^0 in a certain direction e_i^0 , and thus tends to adapt his or her actual velocity v_i with a certain characteristic time τ . Simultaneously, pedestrians i will try to keep a distance from other pedestrians j and walls w by the interaction forces f_{ij} and f_{iw} respectively. Therefore, the velocity

change of pedestrian i in time t can be calculated by the acceleration equation

$$m_i \frac{dv_i}{dt} = m_i \frac{v_i^0(t)e_i^0(t) - v_i(t)}{\tau} + \sum_{j(j \neq i)} f_{ij} + \sum_w f_{iw} \quad (1)$$

where the position change $s_i(t)$ of pedestrian i can be given by the velocity $v_i(t) = ds_i/dt$.

Moreover, the psychological tendency of two pedestrians i and j to stay away from each other can be described by a repulsive interaction force $A_i e^{(r_{ij}-d_{ij})/B_i} n_{ij}$, where A_i and B_i are constants, $d_{ij} = \|s_i - s_j\|$ denotes the center distance between pedestrians i and j , $r_{ij} = (r_i + r_j)$ represents the sum of their radii r_i and r_j , and $n_{ij} = (n_{ij}^1, n_{ij}^2) = (s_i - s_j)/\|s_i - s_j\|$ is the normalized vector pointing from pedestrian j to i . That means the pedestrians will touch each other if their center distance d_{ij} is smaller than their radii sum r_{ij} .

Finally, two additional forces are considered in the social force model, which are body force $k(r_{ij} - d_{ij})n_{ij}$ counteracting body compression and sliding friction force $\kappa(r_{ij} - d_{ij})\Delta v_{ji}^t t_{ij}$ impeding relative tangential motion, respectively. Here $t_{ij} = (-n_{ij}^2, n_{ij}^1)$ is the tangential direction and $\Delta v_{ji}^t = (v_j - v_i)t_{ij}$ means the tangential velocity difference, while k and κ represent corresponding constants.

Therefore, the interaction forces f_{ij} between pedestrians i and pedestrians j can be defined by the equation

$$f_{ij} = A_i e^{(r_{ij}-d_{ij})/B_i} n_{ij} + kg(r_{ij} - d_{ij})n_{ij} + \kappa g(r_{ij} - d_{ij})\Delta v_{ji}^t t_{ij} \quad (2)$$

where the function $g(x)$ is equal to zero if the pedestrians do not touch each other ($r_{ij} < d_{ij}$), and is otherwise equal to the argument x .

Analogously, the corresponding interaction forces f_{iw} with the wall w can also be given by the equation

$$f_{iw} = A_i e^{(r_i-d_{iw})/B_i} n_{iw} + kg(r_i - d_{iw})n_{iw} + \kappa g(r_i - d_{iw})(-v_i t_{iw})t_{iw} \quad (3)$$

in which d_{iw} is the distance to wall w , n_{iw} denotes the direction perpendicular to the wall, and t_{iw} means the direction tangential to the wall, respectively.

2.2. Evacuation scene description

The above-mentioned social force model is employed to simulate the escape panics for 196 pedestrians trying to exit from a $15 \text{ m} \times 20 \text{ m}$ room with a single exit door. The door width was 1.0 m, enough to allow up to two pedestrians to escape simultaneously [28]. The pedestrians are placed in a homogeneously distributed arrangement throughout the $15 \text{ m} \times 15 \text{ m}$ area and this does not exceed healthy indoor environmental regulations [29].

In this work, two qualitatively different obstructing situations were examined, as described in Fig. 1(a) and (b). The former shows a pillar of radius r while the latter corresponds to a thin flat panel of $l \times 0.2 \text{ m}$ size. Moreover, the obstacle–door gap is equal to g and the offset distance of obstacle to the center of the exit is set to p for both pillar-like obstacle and panel-like obstacle. Obviously, only when the offset distance p of obstacle is equal to zero, the obstacle is placed symmetrically. Therefore, from Fig. 1(a) and (b), it is clearly demonstrated that the geometrical parameters of obstacles, including the obstacle size r or l , the obstacle–door gap g and the offset distance p , should be simultaneously optimized in order to achieve a minimum leaving time for all the pedestrians in the room.

Moreover, Fig. 2(a) and (b) presents the desired evacuation directions of pedestrians for pillar-like obstacle and panel-like obstacle. In Fig. 2(a), each pedestrian has a desired evacuation direction pointing to the door. However, for the flat panel in Fig. 2(b), the evacuation direction of pedestrian points to panel's two edges when the pedestrian is behind the panel. Otherwise, it points to the wall in front, until leaving the shadow zone of panel. Outside the shadow zone, pedestrian then has a desired evacuation direction directly pointing to the exit.

Finally, in order to promote the simulated accuracy to the largest degree, the corresponding parameters of social force model are set to $v_0 = 1.48 \text{ m/s}$, $A_i = 998.97 \text{ N}$, $B_i = 0.08 \text{ m}$, $k = 819.62 \text{ kg/s}^2$ and $\kappa = 510.49 \text{ kg/(ms)}$ which refer to our previous literature for escape panics of classroom evacuation in the real-life 2013 Ya'an earthquake in China [30]. Moreover, for each pedestrian, the diameter is 0.6 m, the mass is $m_i = 58 \text{ kg}$, and a reasonable estimate for the acceleration time is $\tau = 0.5 \text{ s}$ in this work.

2.3. Differential evolution algorithm

In this section, a robust differential evolution (DE) is employed to optimize the geometrical parameters of pillar-like and panel-like obstacles in order to achieve an optimal leaving time for all the pedestrians. According to Fig. 1, the three geometrical parameters of obstacles, including the obstacle size r or l , the obstacle–door gap g and the offset distance p , need to be optimized in order to minimize the leaving time for all the pedestrians in the room. In this paper, the optimization range of pillar radius r is $0 \text{ m} \leq r \leq 1.5 \text{ m}$, and the ranges of obstacle–door gap g and offset distance p for pillar-like obstacle are $0 \text{ m} \leq g \leq 2 \text{ m}$ and $-3 \text{ m} \leq p \leq 3 \text{ m}$. Moreover, the optimization range of panel length l is $0 \text{ m} \leq l \leq 14 \text{ m}$, the ranges of obstacle–door gap g and offset distance p for panel-like obstacle are $0 \text{ m} \leq g \leq 4 \text{ m}$ and $-3 \text{ m} \leq p \leq 3 \text{ m}$.

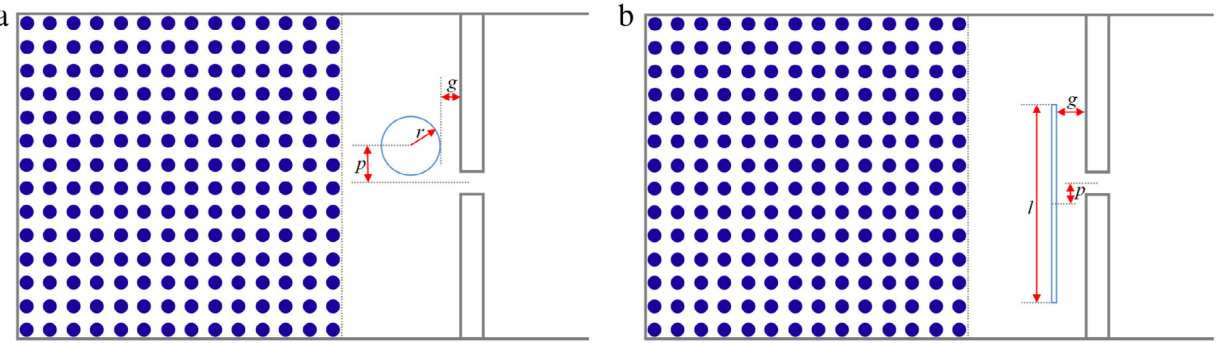


Fig. 1. The geometrical parameters for (a) pillar-like obstacle and (b) panel-like obstacle.

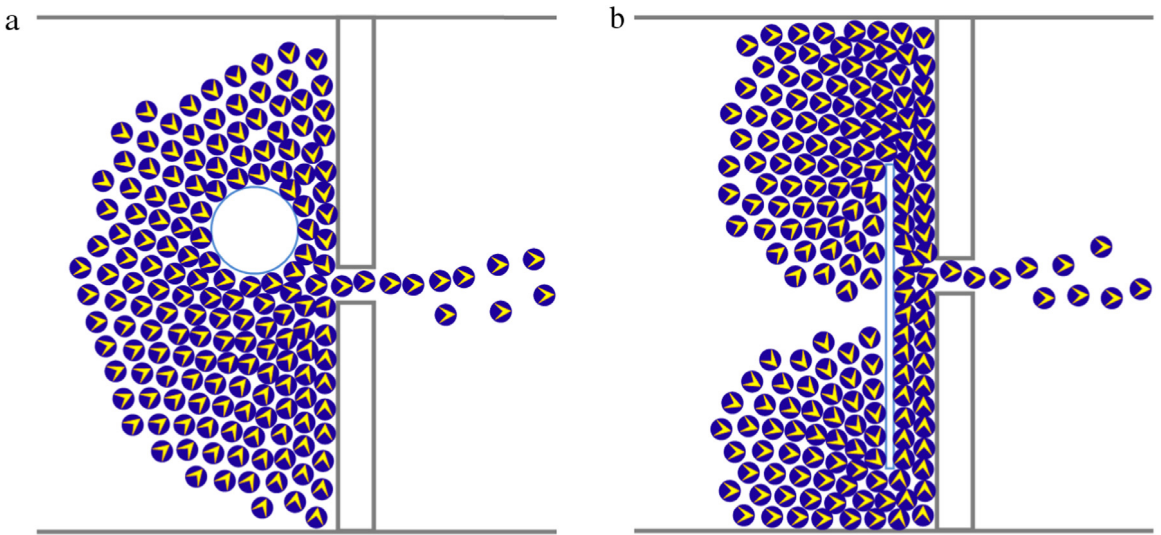


Fig. 2. The desired evacuation directions of pedestrians for (a) pillar-like obstacle and (b) panel-like obstacle.

respectively. Obviously, these geometrical variables r or l , g and p are highly correlated with each other, hence they should not be analyzed and optimized separately but be considered all together in order to obtain the global optimal solution.

Heuristic search techniques like Genetic Algorithms [20,31] and Genetic Programming [32] have been successfully applied to many complex optimization problems to pursue novel solutions that are difficult to obtain using the conventional approaches. Differential Evolution (DE) algorithm [30,33,34] is a new heuristic approach which mainly has three advantages: finding the true global optimal solution regardless of the initial parameter values, fast convergence, and using few control parameters such as population size, scale factor, crossover rate, crossover strategy and maximum generations. Therefore, in this paper, the differential evolution algorithm is introduced to optimize the geometrical parameters of pillar-like and panel-like obstacles to obtain a minimum leaving time for all the pedestrians. The DE algorithm uses mutation operation as a search mechanism and selection operation to direct the search toward the prospective regions in the search space. The DE algorithm also uses a non-uniform crossover that can take child vector parameters from one parent more often than it does from others. By using the components of the existing population members to construct trial vectors, the recombination (crossover) operator efficiently uses information about successful combinations, thus enabling the search for a better solution space.

The block diagram of the DE-based geometrical parameters optimization for pillar-like and panel-like obstacles is illustrated in Fig. 3. Firstly, an initial population is generated randomly. Then the three geometrical parameters (r , g and p for pillar-like obstacle, or l , g and p for panel-like obstacle) of each individual are generated for evacuation simulation using social force model. The fitness function is then calculated based on the evacuation simulation results. The DE judges if the termination criteria is met. If not, the population is regenerated through a DE process including selection, crossover and mutation. In this paper, the exponential crossover strategy of DE/rand-to-best/1/exp is applied in the DE. The DE process is repeated until the maximum number of the generation is reached.

The goal of DE is to pursue the optimal geometrical parameters of pillar-like and panel-like obstacles in order to minimize the leaving time for all the pedestrians in the room. Therefore, the fitness function F of DE for pillar-like obstacle can be

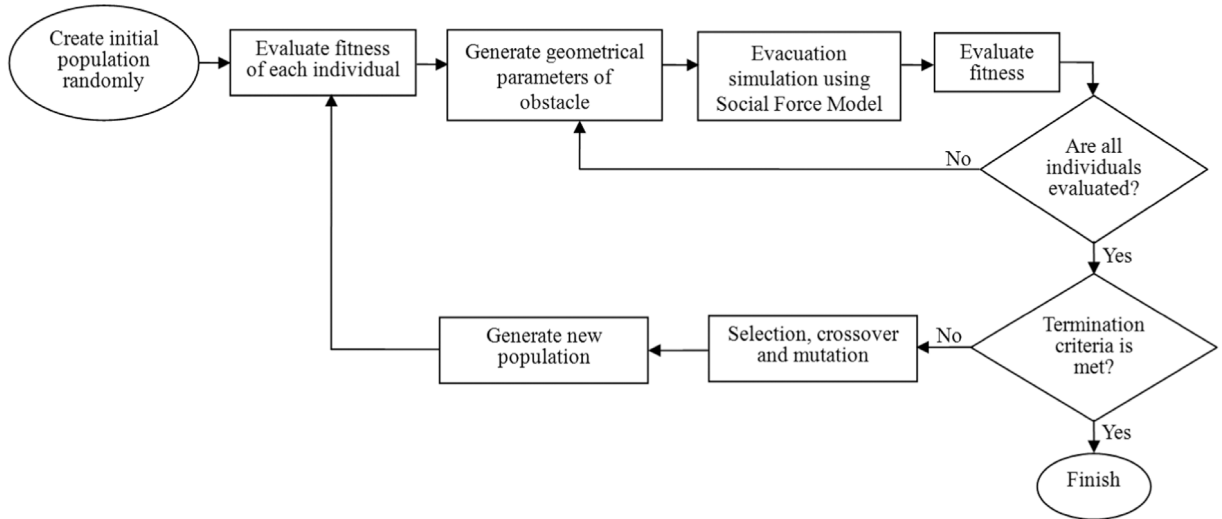


Fig. 3. The block diagram of the DE-based geometrical parameters optimization for pillar-like and panel-like obstacles.

Table 1
Parameters for the DE optimization.

Population size	30
Scale factor	0.5
Crossover rate	0.2
Crossover strategy	DE/rand-to-best/1/exp
Maximum generations	300

defined as follows:

$$\text{Minimize: } F = T_{\text{pillar}} \quad (4)$$

$$\text{Subject to: } 0 \text{ m} \leq r \leq 1.5 \text{ m} \quad (5)$$

$$0 \text{ m} \leq g \leq 2 \text{ m} \quad (6)$$

$$-3 \text{ m} \leq p \leq 3 \text{ m.} \quad (7)$$

In the formula (4), the T_{pillar} denotes the leaving time for all the pedestrians in the room when a pillar-like obstacle is placed in front of the exit. The r represents the radius of pillar, the g is the closest obstacle–door gap, and the p is the offset distance of obstacle to the center of the exit.

Similarly, the fitness function F of DE for panel-like obstacle can be defined as follows:

$$\text{Minimize: } F = T_{\text{panel}} \quad (8)$$

$$\text{Subject to: } 0 \text{ m} \leq l \leq 14 \text{ m} \quad (9)$$

$$0 \text{ m} \leq g \leq 4 \text{ m} \quad (10)$$

$$-3 \text{ m} \leq p \leq 3 \text{ m.} \quad (11)$$

In the formula (8), the T_{panel} denotes the leaving time for all the people when a panel-like obstacle is placed in front of the exit. The l represents the length of panel, the g is also the closest obstacle–door gap, and the p is the offset distance of panel obstacle to the center of the door respectively.

The parameters for the DE optimization are listed in Table 1. The DE optimization experiments in this work were executed under Microsoft Windows Server 2003 with 3.00 GHz of Intel(R) Pentium(R) 4 CPU and 2 GB of RAM.

The convergence curves of DE for geometrical parameters optimization of panel-like obstacle are presented in Fig. 4. With the increase of the generation from 1 to 300, the objective function F of DE for panel-like obstacle is getting smaller and smaller which decreases from 97.48 to 77.95 s. Fig. 4 clearly demonstrates that the differential evolution algorithm almost converges before the maximum number of the generation is reached.

2.4. Optimization results and discussion

The optimal geometrical parameters for pillar-like obstacle and panel-like obstacle are listed in Table 2. From Table 2 it can be clearly seen that the objective function F is equal to 101.1 s when there is no obstacle in front of the exit. However, when the geometrical parameters of pillar-like obstacle are set to $r = 1.38 \text{ m}$, $g = 0.97 \text{ m}$, $p = 1.20 \text{ m}$, the objective

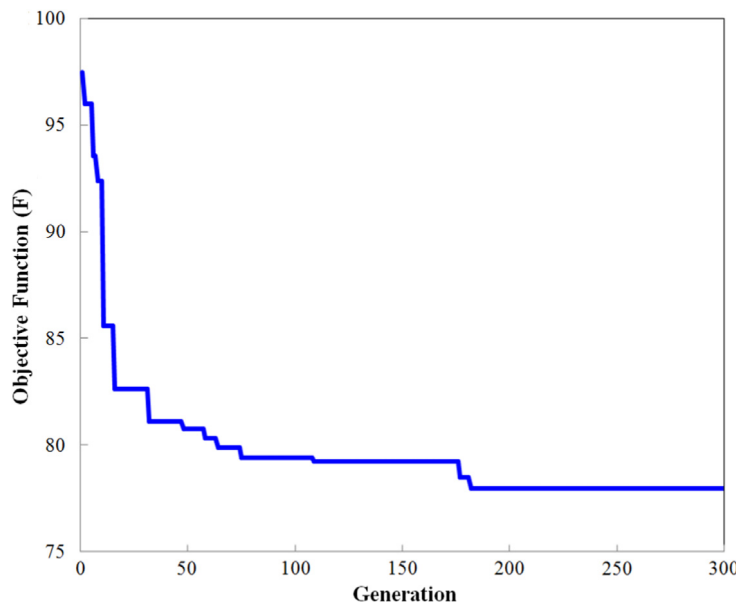


Fig. 4. The convergence curves of DE for geometrical parameters optimization of panel-like obstacle.

Table 2

The optimal geometrical parameters of obstacles.

Obstacle type	Objective function F	Optimal geometrical parameters
No obstacle	101.1 s	
Pillar-like obstacle	92.39 s	$r = 1.38 \text{ m}, g = 0.97 \text{ m}, p = 1.20 \text{ m}$
Panel-like obstacle	77.95 s	$l = 11.68 \text{ m}, g = 1.08 \text{ m}, p = -0.15 \text{ m}$

function F has been decreased to 92.39 s. Similarly, when the geometrical parameters of panel-like obstacle are set to $l = 11.68 \text{ m}, g = 1.08 \text{ m}$ and $p = -0.15 \text{ m}$, the objective function F can also be improved to $F = 77.95 \text{ s}$. Therefore, with the optimal geometrical parameters optimized by differential evolution algorithm, the leaving time of 101.1 s for all the pedestrians has been reduced to 92.39 s and 77.95 s respectively when suitably placing a pillar-like obstacle and a panel-like obstacle in front of the exit.

Moreover, in order to analyze and compare the different evacuation performance for no obstacle, pillar-like obstacle and panel-like obstacle, the number of evacuated people at different evacuation time is depicted in Fig. 5.

Fig. 5 clearly demonstrates that the evacuated people number of panel-like obstacle at different evacuation time is obviously superior to that of pillar-like obstacle and no obstacle. The evacuation speed curve of panel-like obstacle is near linear because of orderly evacuation of pedestrians from the room under the insulation and guidance of the panel obstacle. However, the pedestrian evacuation speed of pillar-like obstacle and no obstacle is typically nonlinear which is getting slower and slower due to the congestion in the crowd. The evacuation speed curve of pillar-like obstacle is broadly consistent with that of no obstacle before the evacuation time of $t = 71 \text{ s}$, but the evacuation efficiency of pillar-like obstacle is better than that of no obstacle after the evacuation time of $t = 71 \text{ s}$. Especially, the evacuated people number of panel-like obstacle is slightly less than that of pillar-like obstacle and no obstacle before the evacuation time of $t = 25 \text{ s}$ because the pedestrians need to walk a longer distance to reach the door when placing a panel-like obstacle in front of the exit.

To sum up, both pillar-like obstacle and panel-like obstacle can decrease the leaving time for all the pedestrians and thus enhance the evacuation efficiency when suitably placing a pillar or panel in front of the exit. Therefore, the geometrical parameters' optimization methodology presented in this paper that uses a social force model optimized by differential evolution technique is a very convenient and efficient way to pursue an optimal obstacle layout in order to obtain a maximum enhancement of evacuation performance.

3. Effects of obstacle layout on evacuation efficiency

In order to understand the sensitiveness of obstacle parameters, the effects of these geometrical parameters of obstacles on evacuation time have been further analyzed respectively, including the size of obstacle r or l , the obstacle–door gap g and the offset distance p of obstacle to the center of the exit, which are depicted in Figs. 6 and 7.

From the results of Fig. 6, it is seen that all the three geometrical parameters of pillar-like obstacle could markedly influence the objective function F or the leaving time T_{pillar} for all the pedestrians in the room. In Fig. 6(a), the parameter

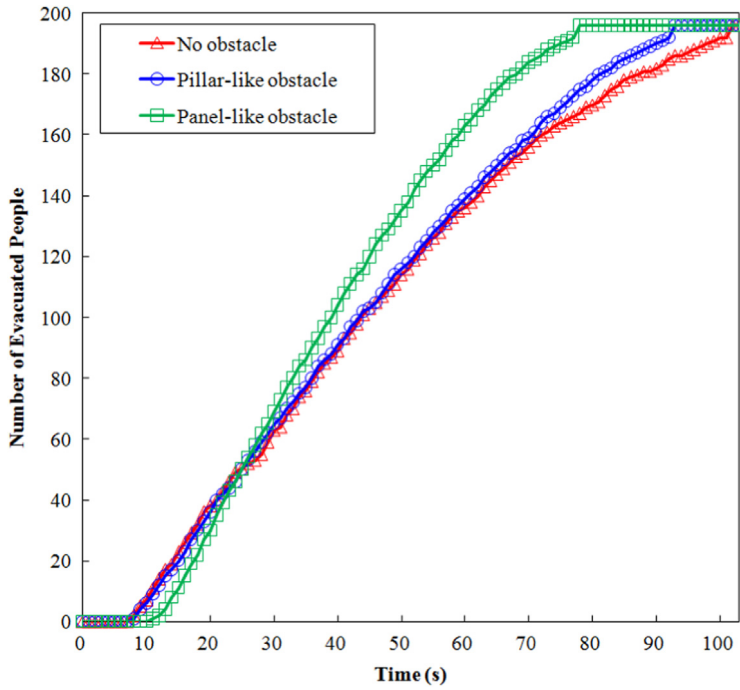


Fig. 5. The evacuated people comparison among no obstacle, pillar-like obstacle and panel-like obstacle respectively at different evacuation time.

range of pillar radius is $0 \text{ m} \leq r \leq 1.5 \text{ m}$, and other geometrical parameters of pillar-like obstacle are set to $g = 0.97 \text{ m}$ and $p = 1.20 \text{ m}$. It is clearly demonstrated that with the increase of pillar radius r from 0 to 1.5 m, the objective function F fluctuates periodically between about 100 and 110 s. Only when the pillar radius r is equal to 1.38 m, the objective function F can reach its lowest value. Therefore, it would be hard to achieve the global optimal solution by manual adjustment of geometrical parameters because of the multimodality of objective function F . Moreover, in Fig. 6(b), the parameter range of obstacle–door gap is $0 \text{ m} \leq g \leq 2 \text{ m}$, and other geometrical parameters of pillar-like obstacle are set to $r = 1.38 \text{ m}$ and $p = 1.20 \text{ m}$. From Fig. 6(b), it can be seen that with the increase of obstacle–door gap g from 0 to 2 m, the objective function F firstly reduces remarkably, and achieves its minimum values when obstacle–door gap g is equal to 0.97 m, then fluctuates with a rising trend.

Finally, according to Fig. 6(c), it is obviously seen that when the offset distance p of obstacle to the center of the exit is equal to zero, which means the pillar-like obstacle is placed symmetrically, the evacuation performance almost becomes the worst. This findings are consistent with results of extant literature [26,27] in which it will be harmful and inefficient for obstacles placed symmetrically near the exit door. With the increase of offset distance p from 0 to 3 m, the objective function F firstly decreases and reaches the optimal values when offset distance p is 1.20 m, then it begins to increase. Moreover, with the decrease of offset distance p from 0 to -3 m, the objective function F also decreases and achieves its minimum values, then it begins to fluctuate with a rising trend. Obviously, the best way for achieving an optimal evacuation performance is to shift the pillar-like obstacle about 1.20 m from the center of the exit.

Similarly, according to Fig. 7, it is clearly seen that there exists optimum value of obstacle length l , obstacle–door gap g and offset distance p for panel-like obstacle. Firstly, in Fig. 7(a), the parameter range of panel length is $0 \text{ m} \leq l \leq 14 \text{ m}$, and other geometrical parameters of panel-like obstacle are set to $g = 1.08 \text{ m}$ and $p = -0.15 \text{ m}$. With the increase of obstacle length l from 0 to 14 m, the objective function F firstly increases, then starts to decreases continuously, and achieves the optimal values of 77.95 s when the obstacle length l is equal to 11.68 m. Moreover, when the obstacle length l exceeds 11.68 m, the objective function F begins to increase dramatically. Fig. 7(b) reveals that with the increase of obstacle–door gap g from 0 to 4 m, the objective function F or the leaving time T_{panel} for all the pedestrians firstly reduces dramatically, and obtains its optimal values when obstacle–door gap g is 1.08 m, then it starts to fluctuate with an increasing tendency.

At last, in Fig. 7(c), the parameter range of offset distance p is $-1 \text{ m} \leq p \leq 1 \text{ m}$, and other parameters of obstacle are fixed to $l = 11.68 \text{ m}$ and $g = 1.08 \text{ m}$. Totally different from the conclusion of pillar-like obstacle, when the offset distance p of panel-like obstacle is equal to zero, the objective function F or the evacuation time T_{panel} for all the pedestrians is not the worst. However, to achieve the optimal evacuation performance, the offset distance p should be equal to -0.15 m. That means we should shift the panel-like obstacle slightly from the center of the exit in order to enhance the pedestrian outflow to the most degree.

To sum up, the geometrical parameters of obstacles are actually highly correlated with each other, and should not be optimized separately but be considered all together in order to obtain the global optimal value of objective function. It is

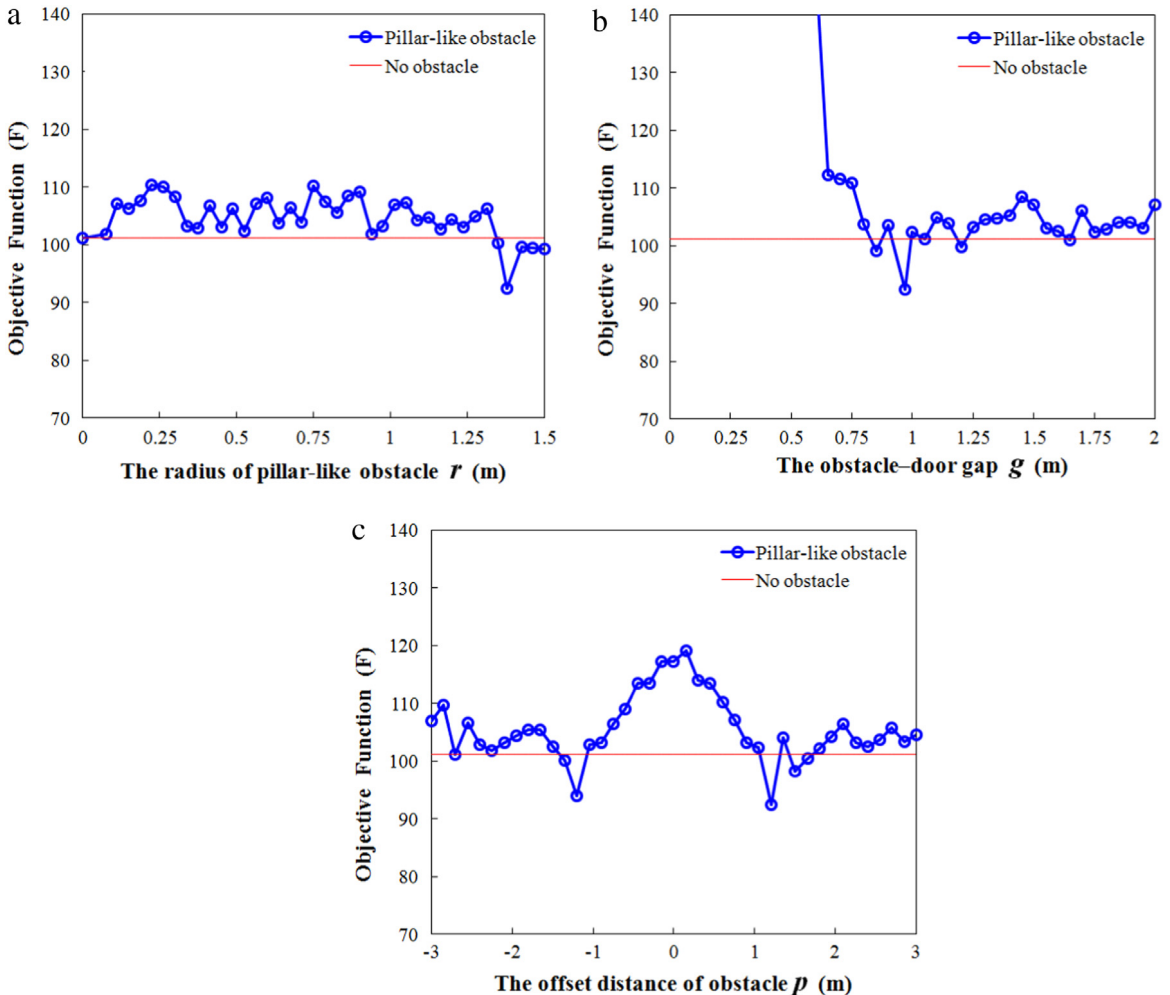


Fig. 6. The effects of (a) the radius of obstacle r , (b) the obstacle–door gap g and (c) the offset distance of obstacle p on objective function F of pillar-like obstacle, respectively.

also demonstrated that all the geometrical parameters of obstacles have remarkable influence upon the objective function, and the evacuation performances of pillar-like and panel-like obstacles are quite sensitive to these geometrical parameters.

Especially, from Figs. 6 and 7, it is clearly demonstrated the effective geometrical parameter ranges for pillar-like obstacle are quite narrow and limited to enhance the evacuation performance compared to no obstacle. However, the effective geometrical parameter ranges for panel-like obstacle are relatively broad. That means, the panel-like obstacle is actually more robust and stable than the pillar-like obstacle to guarantee the enhancement of evacuation performance.

4. Profiles analysis of density, velocity and specific flow

In this section, in order to investigate the physical mechanism of evacuation performance enhancement, the profiles of density, velocity and specific flow for no obstacle, pillar-like obstacle and panel-like obstacle are compared in detail based on the Voronoi method.

Fig. 8 depicts the simulated pedestrian trajectories for no obstacle, pillar-like obstacle and panel-like obstacle in which the geometrical parameters of pillar-like obstacle are set to $r = 1.38$ m, $g = 0.97$ m and $p = 1.20$ m, and the parameters of panel-like obstacle are fixed to $l = 11.68$ m, $g = 1.08$ m and $p = -0.15$ m respectively based on the optimization results of differential evolution algorithm. Moreover, the interval of collecting data in the simulation are all set to 0.1 s. As shown in Fig. 8, the evacuation processes of pedestrians have changed tremendously after placing an obstacle in front of the exit. In particular, when placing a panel-like obstacle in front of the door, the pedestrians must firstly move to the panel's two edges in order to leave the shadow zone of panel as early as possible, then begin to rush into the exit from two different channel entrances.

By using pedestrian trajectories with high precision, the profiles of density, velocity and specific flow for no obstacle, pillar-like obstacle and panel-like obstacle can be further analyzed. In this study, the Voronoi method is employed to

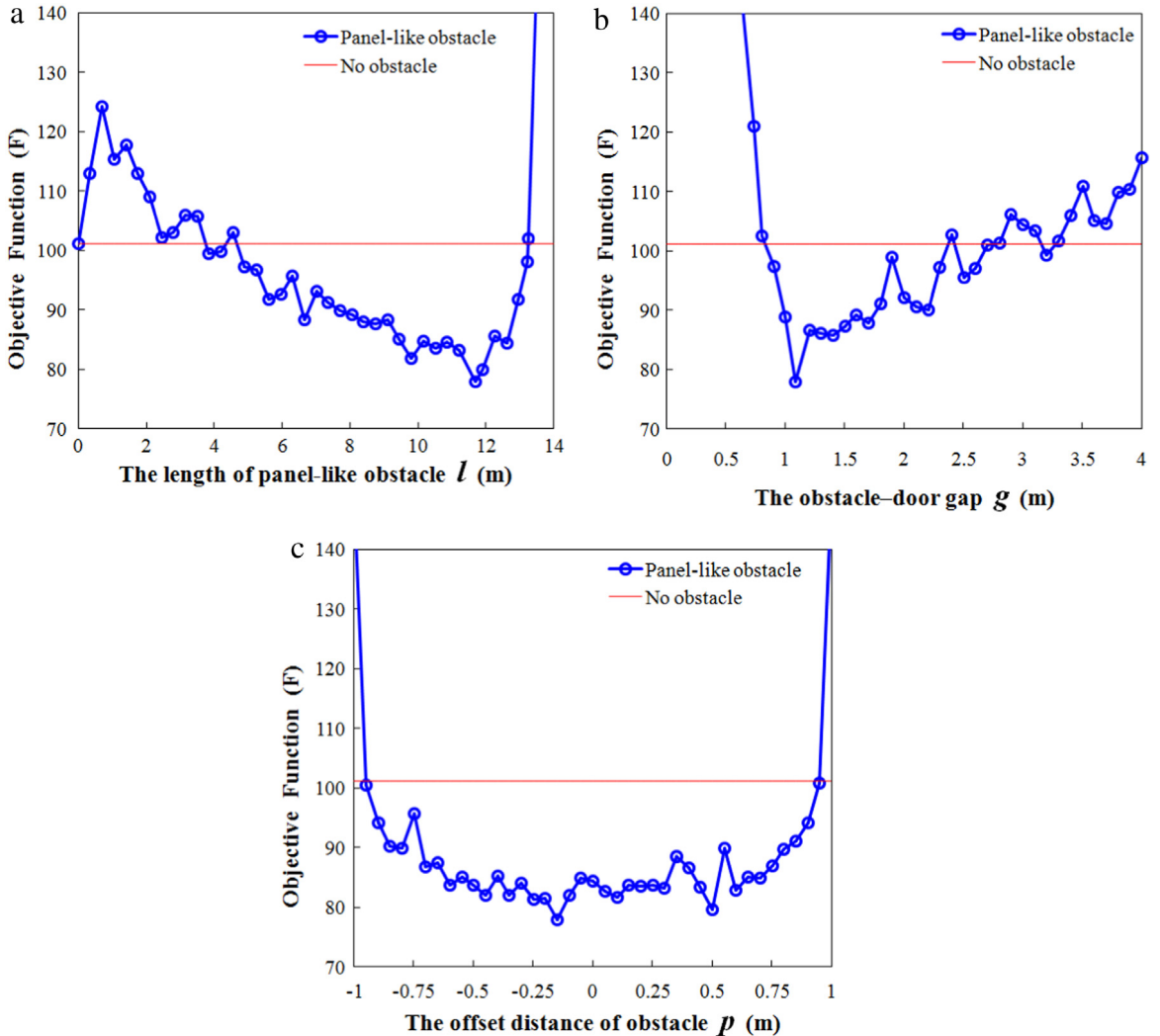


Fig. 7. The effects of (a) the length of obstacle l , (b) the obstacle–door gap g and (c) the offset distance of obstacle p on objective function F of panel-like obstacle, respectively.

calculate the corresponding density, velocity, and flow because it is able to produce a good resolution in time and space in combination with reduced fluctuations.

The idea of the Voronoi diagram is to allocate every point, in our case the position of every pedestrian, the area closer to this point than to any other one. Thus for every Voronoi cell the area A_i can be obtained and the density as well as velocity distribution $\rho_{x,y}$ and $v_{x,y}$ can be determined. Definitions of quantities are taken from Refs. [35,36]:

$$\rho_{x,y} = \frac{1}{A_i} \quad \text{and} \quad v_{x,y} = v_i(t) \quad \text{if } (x, y) \in A_i, \quad (12)$$

where $v_i(t)$ is the simulated instantaneous velocity of each pedestrian.

Therefore, the corresponding Voronoi mean density $\bar{\rho}$ for the measurement area can be defined as:

$$\bar{\rho} = \frac{\iint \rho_{x,y} dx dy}{\Delta x \cdot \Delta y}. \quad (13)$$

Δx is the length and Δy is the width of the measurement areas. Similarly, the Voronoi mean velocity \bar{v} can be defined as:

$$\bar{v} = \frac{\iint v_{x,y} dx dy}{\Delta x \cdot \Delta y}. \quad (14)$$

The measurement areas we used to calculate the profiles of density, velocity and specific flow are set to $\Delta x = 20$ m ($0 \leq x \leq 20$ m) and $\Delta y = 15$ m ($0 \leq y \leq 15$ m) for indoor room, and $\Delta x = 6$ m ($20 \leq x \leq 26$ m) and $\Delta y = 15$ m ($0 \leq y \leq 15$ m) for outdoor area respectively.

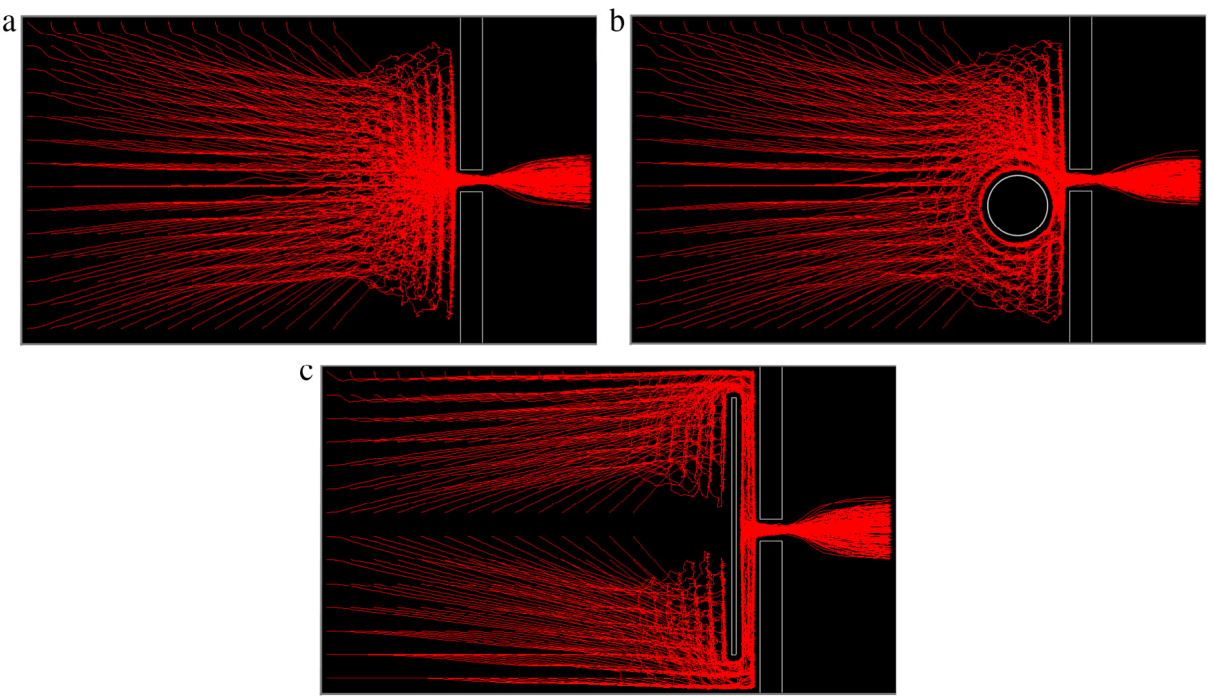


Fig. 8. The pedestrian trajectories for (a) no obstacle, (b) pillar-like obstacle and (c) panel-like obstacle.

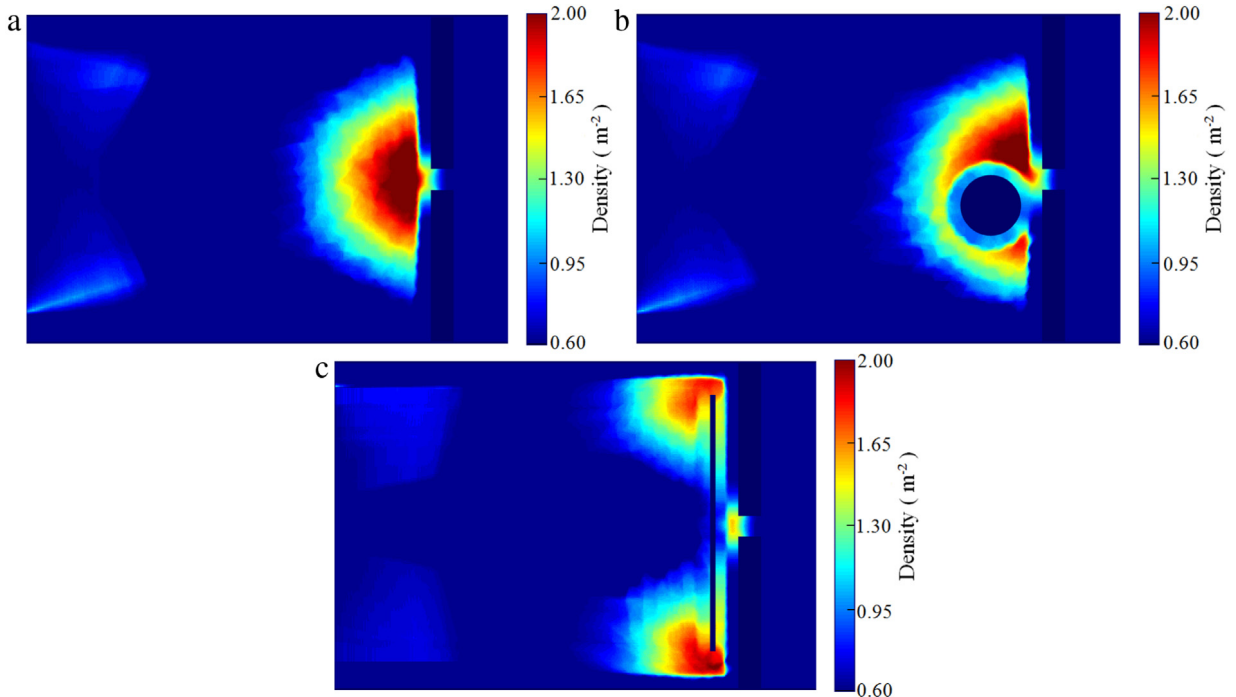


Fig. 9. The density profiles for (a) no obstacle, (b) pillar-like obstacle and (c) panel-like obstacle. (For interpretation of the references to color in this figure legend, the reader is referred to the web version of this article.)

The Voronoi method offers the possibility to measure areas smaller than pedestrians, therefore, we divided the complete geometry in 5 cm squares in this study, and the densities and velocities are calculated for every square. Figs. 9–11 demonstrate the corresponding profiles of density, velocity and specific flow for no obstacle, pillar-like obstacle and panel-like obstacle respectively based on the proposed Voronoi method.

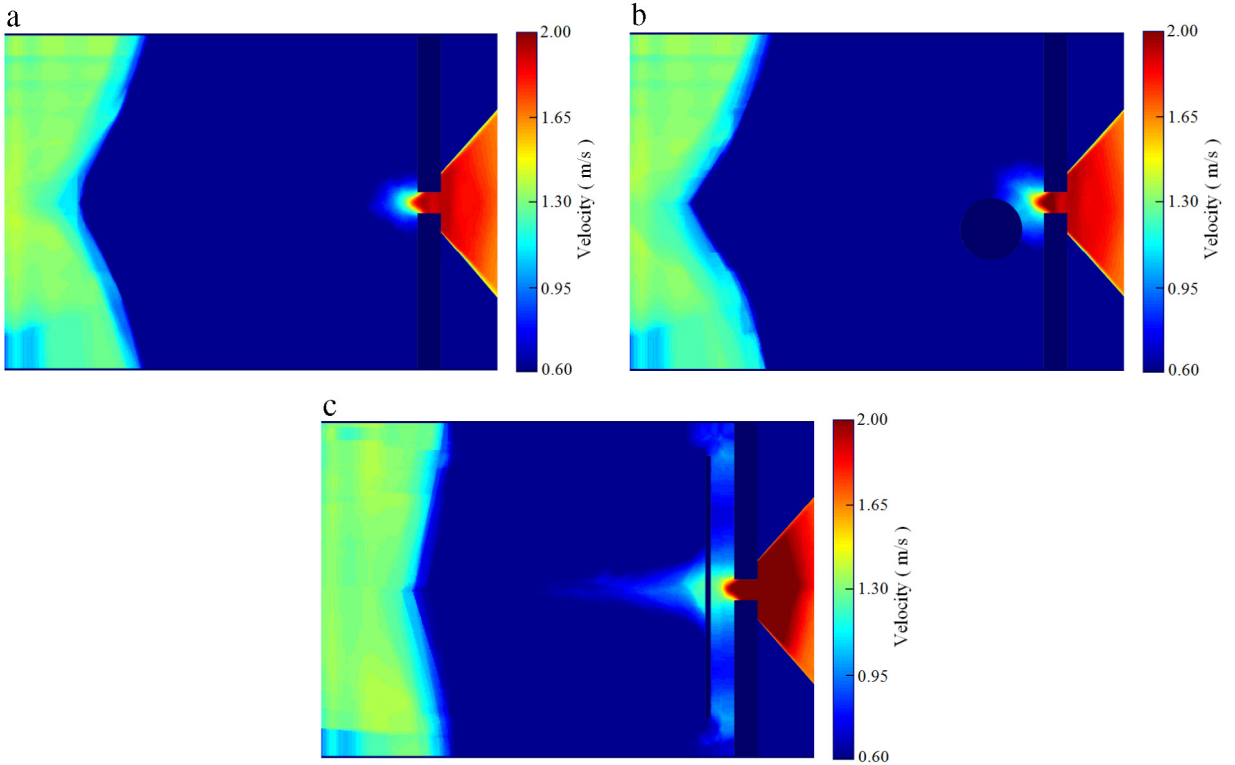


Fig. 10. The velocity profiles for (a) no obstacle, (b) pillar-like obstacle and (c) panel-like obstacle. (For interpretation of the references to color in this figure legend, the reader is referred to the web version of this article.)

From Fig. 9, it can be clearly seen that the density profiles of pedestrians have changed significantly when placing an obstacle in front of the exit. Firstly, in Fig. 9(a), the high density of above 2.0 m^{-2} (dark red area) appears around exit zone because all the pedestrians rush into the exit directly when evacuation begins. Secondly, in Fig. 9(b), the high density area of above 2.0 m^{-2} decreases remarkably when placing a pillar in front of the exit because the pedestrians need to bypass a pillar obstacle when passing through the exit. Finally, it can be clearly seen from Fig. 9(c) that the dark red high density area of above 2.0 m^{-2} almost disappears completely when placing a panel-like obstacle in front of the exit. People need to firstly rush into the panel's two edges after placing a panel-like obstacle in front of the door, therefore, the maximum densities are apparent at two edges of the panel.

On the whole, the indoor maximum density ρ_{\max} reaches 2.2 m^{-2} , and the average density $\bar{\rho}$ is 1.0 m^{-2} for no obstacle. When placing a pillar obstacle with optimal layout in front of the exit, the indoor maximum density ρ_{\max} and average density $\bar{\rho}$ both decrease to 2.15 m^{-2} and 0.96 m^{-2} respectively. Furthermore, when placing an optimal panel-like obstacle in front of the exit, the corresponding indoor maximum density ρ_{\max} and average density $\bar{\rho}$ further reduce to 2.02 m^{-2} and 0.95 m^{-2} . That is to say, the high density region of above 2.0 m^{-2} near the exit has been significantly reduced by effective separation in space when placing an obstacle in front of the exit, especially for the panel-like obstacle. Additionally, according to Fig. 9(a)–(c), it is clearly seen that there all exist two higher density areas with light blue color on the left for no obstacle, pillar-like obstacle and panel-like obstacle which are formed owing to the fact that all the initial pedestrians on the left immediately run with a desired evacuation direction pointing to the exit on the right when the evacuation commences.

Similarly, Fig. 10 shows the corresponding velocity profiles for no obstacle, pillar-like obstacle and panel-like obstacle. The velocity area of above 0.95 m/s (light blue area) around exit zone gradually increase when placing a pillar-like obstacle and a panel-like obstacle in front of the door. In particular, almost the whole channel region between the panel and the wall in front has a speed of above 0.95 m/s . In Fig. 10(a), the maximum velocity v_{\max} for indoor room achieves 1.87 m/s , and the average velocity \bar{v} is 0.39 m/s when there is no obstacle in front of the exit. However, in Fig. 10(b), the maximum velocity v_{\max} and average velocity \bar{v} both improve to 1.99 m/s and 0.42 m/s , and in Fig. 10(c), the maximum velocity v_{\max} and average velocity \bar{v} further rise to 2.13 m/s and 0.6 m/s respectively. Moreover, the velocity region of above 2.0 m/s (dark red region) for outdoor area also increases when placing an obstacle in front of the door. Especially for the panel-like obstacle, nearly the whole outdoor area is dark red with a high escape speed of above 2.0 m/s . That means the original outdoor maximum velocity v_{\max} of 1.94 m/s and average velocity \bar{v} of 1.03 m/s for no obstacle have also been improved to 2.04 m/s and 1.07 m/s for pillar-like obstacle, and further enhanced to 2.25 m/s and 1.33 m/s respectively for panel-like obstacle.

In addition, from Fig. 10(a)–(c), it is clearly demonstrated that the higher velocity areas with green color are quite apparent on the left for no obstacle, pillar-like obstacle and panel-like obstacle because all the initial people on the left can

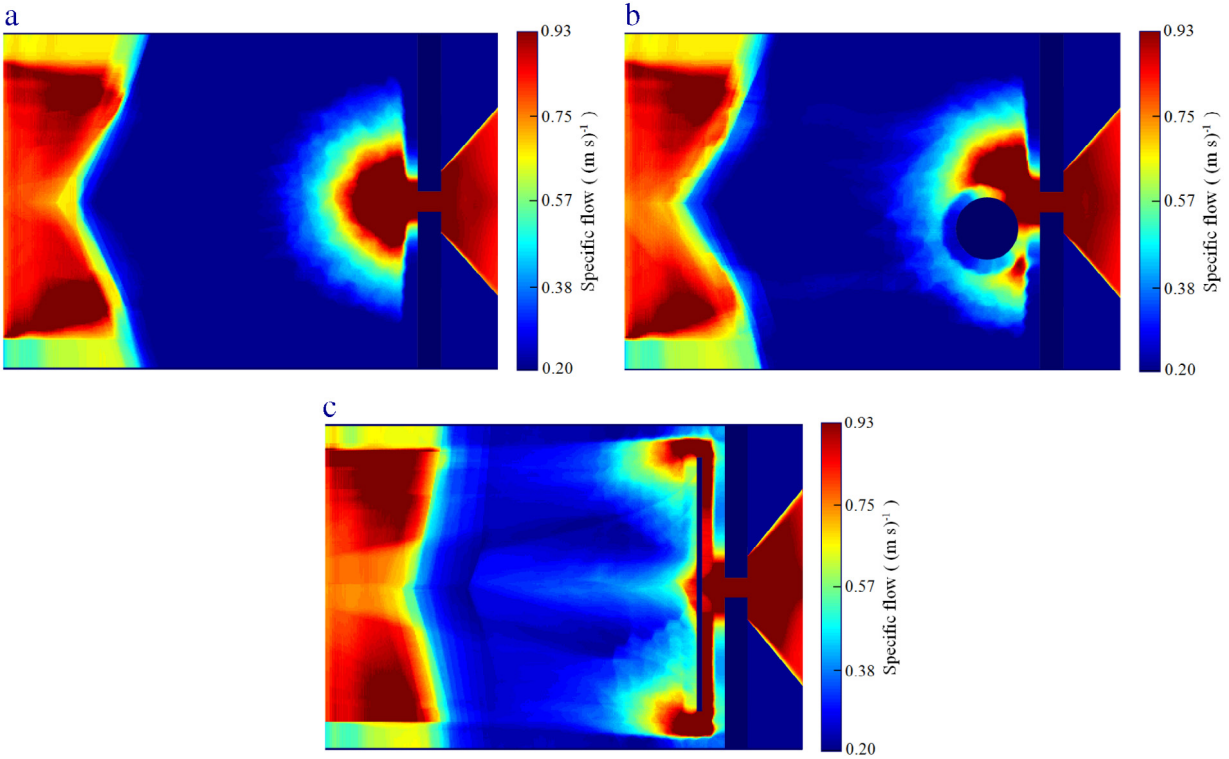


Fig. 11. The specific flow profiles for (a) no obstacle, (b) pillar-like obstacle and (c) panel-like obstacle. (For interpretation of the references to color in this figure legend, the reader is referred to the web version of this article.)

run with a desired velocity of $v_0 = 1.48 \text{ m/s}$ when the evacuation begins, however, the evacuation velocity of pedestrians will gradually slow down as a result of increasing crowd density when all the pedestrians start to converge on the exit. Finally, we can also find that the maximum evacuation velocities v_{\max} of pedestrians for outdoor area are 1.94 m/s , 2.04 m/s and 2.25 m/s respectively for no obstacle, pillar-like obstacle and panel-like obstacle which all significantly exceed the desired velocity of $v_0 = 1.48 \text{ m/s}$ because when passing through the exit, pedestrians have undergone a higher body force from others which will cause the instantaneously rising of escape speed.

Lastly, specific flow profiles are calculated by the product of the corresponding density and velocity cells based on $J = \rho \cdot v$. It can be clearly seen from Fig. 11 that the specific flow profiles are completely inhomogeneous for no obstacle, pillar-like obstacle and panel-like obstacle. The highest specific flow values are all located at the left of the indoor room, the region near the exit door, and the outdoor area. The highest flows observable on the left and in the outdoor area are both formed because of the high evacuation velocities on the left and in the outdoor area which can be clearly found in Fig. 10. Moreover, the highest specific flow distributions in the indoor region near the exit are basically in accord with the high density distributions near the exit which are presented in Fig. 9.

From Fig. 11(a)–(c), it is clearly demonstrated that the maximum specific flow J_{\max} and average specific flow \bar{J} for indoor room and outdoor area both achieve significant enhancement after placing a pillar-like or panel-like obstacle. For example, the original indoor maximum specific flow J_{\max} of 2.5 (m s)^{-1} and average specific flow \bar{J} of 0.44 (m s)^{-1} for no obstacle have been increased to 2.71 (m s)^{-1} and 0.45 (m s)^{-1} for pillar-like obstacle, and further enhanced to 2.97 (m s)^{-1} and 0.55 (m s)^{-1} respectively for panel-like obstacle. Especially, for panel-like obstacle, the specific flow of lower channel is obviously higher than that of upper channel because almost the whole lower channel along the panel has high specific flow of above 0.93 (m s)^{-1} (dark red area), however, only half of upper channel along the panel has dark red high flow of above 0.93 (m s)^{-1} . This is because the optimal panel obstacle is placed asymmetrically with a slight upper shift which leads to relatively clogging near the entrance of upper channel.

Furthermore, for outdoor area, the original outdoor maximum outflow J_{\max} of 2.26 (m s)^{-1} and average outflow \bar{J} of 0.54 (m s)^{-1} for no obstacle have also been improved to 2.54 (m s)^{-1} and 0.56 (m s)^{-1} for pillar-like obstacle, and further increased to 2.91 (m s)^{-1} and 0.7 (m s)^{-1} for panel-like obstacle. It is clear from Fig. 11 that the high outflow region of above 0.93 (m s)^{-1} (dark red area) for outdoor area is getting bigger and bigger when placing a pillar-like obstacle and a panel-like obstacle. In particular, when placing a panel-like obstacle in front of the door, nearly the whole outdoor area has a dark red high outflow of above 0.93 (m s)^{-1} .

To sum up, the above profiles' analyses of density, velocity and specific flow demonstrate that the physical mechanism behind the evacuation performance enhancement while placing an obstacle is a direct decrease of high density region by

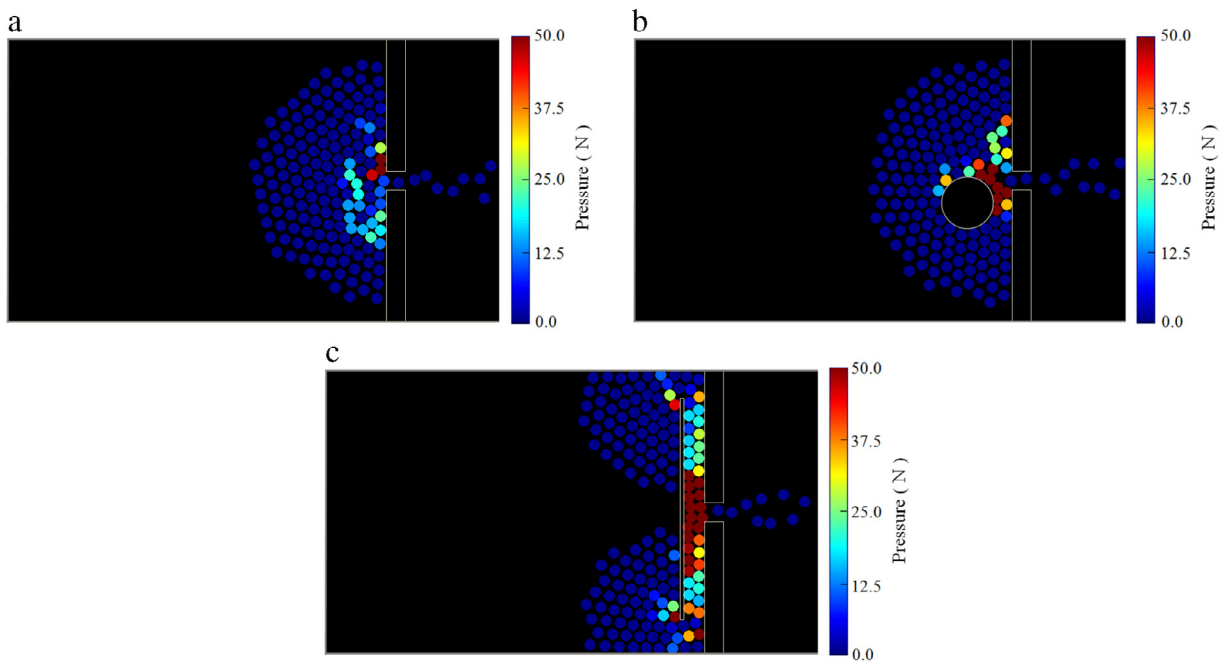


Fig. 12. The pedestrian instantaneous pressures for (a) no obstacle, (b) pillar-like obstacle and (c) panel-like obstacle respectively at the evacuation time of $t = 15$ s. (For interpretation of the references to color in this figure legend, the reader is referred to the web version of this article.)

effective separation in space which causes the dramatic increase of escape speed and evacuation outflow. In this work, the maximum outflow J_{\max} and average outflow \bar{J} for outdoor area have been improved by 12.39% and 3.70% when placing a pillar-like obstacle with optimal layout. Furthermore, the corresponding maximum outflow J_{\max} and average outflow \bar{J} has been further enhanced by 28.76% and 29.63% respectively when placing an optimal panel-like obstacle in front of the exit. Therefore, compared to the pillar-like obstacle, the panel-like obstacle can more significantly decrease the high density region by effective separation in space, and increase the escape speed of pedestrians near the area of exit which finally leads to the more remarkable enhancement of pedestrian outflow.

5. Spatial distribution analysis of crowd pressures

To investigate whether placing an obstacle can reduce the pressure in the region of exit or, on the contrary, increase the pressure to a more dangerous level, the maximum pressure, the average pressure, and the spatial distribution of pedestrian pressures among no obstacle, pillar-like obstacle and panel-like obstacle are analyzed in detail in this section. Fig. 12 depicts the pedestrian instantaneous pressures for no obstacle, pillar-like obstacle and panel-like obstacle respectively at the evacuation time of $t = 15$ s. In this work, the instantaneous pressures of pedestrians are defined as the sum of the magnitudes of the radial forces acting on them.

The circles in Fig. 12(a)–(c) are the corresponding locations of pedestrians at the evacuation time of $t = 15$ s, and the colors identify the pedestrian instantaneous pressures. For example, a dark red indicates a higher pressure, while a dark blue indicates a lower pressure. From Fig. 12(a), it can be clearly seen that only two pedestrians close to wall have a higher pressure with dark red color for no obstacle scene. However, in Fig. 12(b), seven pedestrians have been congested between pillar and exit with a higher pressure of dark red when placing a pillar-like obstacle in front of the exit. Furthermore, nearly half of pedestrians in the channel between panel and wall have obvious body collisions with each other which results in a higher physical pressure force with dark red color in the middle of panel channel as shown in Fig. 12(c).

In this work, the pedestrian instantaneous pressures at any moment along the whole trajectory of a pedestrian from indoor room to outdoor area can be recorded. Therefore, the overall spatial distributions of pedestrian pressures for no obstacle, pillar-like obstacle and panel-like obstacle can be graphed in Fig. 13 by interpolating these force-points. To make the features of pedestrian pressure distributions more obvious, the upper limit of pressure color bar is set to 50 N.

From Fig. 13, it is clearly demonstrated that the spatial distributions of pedestrian pressures are all inhomogeneous for no obstacle, pillar-like obstacle and panel-like obstacle. In Fig. 13(a), the high pedestrian pressure of above 50 N (dark red area) are mainly concentrated at the two sides of the wall close to exit. However, in Fig. 13(b), besides the high pressure at the two sides of the wall close to door, there also exists an obvious high pressure region of above 50 N with dark red color between the pillar and the wall in front because of the body conflicts of pedestrians in a relative enclosed space. Especially, in Fig. 13(c), besides the high pressure along the panel and the wall in front, a larger high pressure region of above 50 N with dark red color appears at the center of the channel between the panel and the wall in front because the pedestrians at the

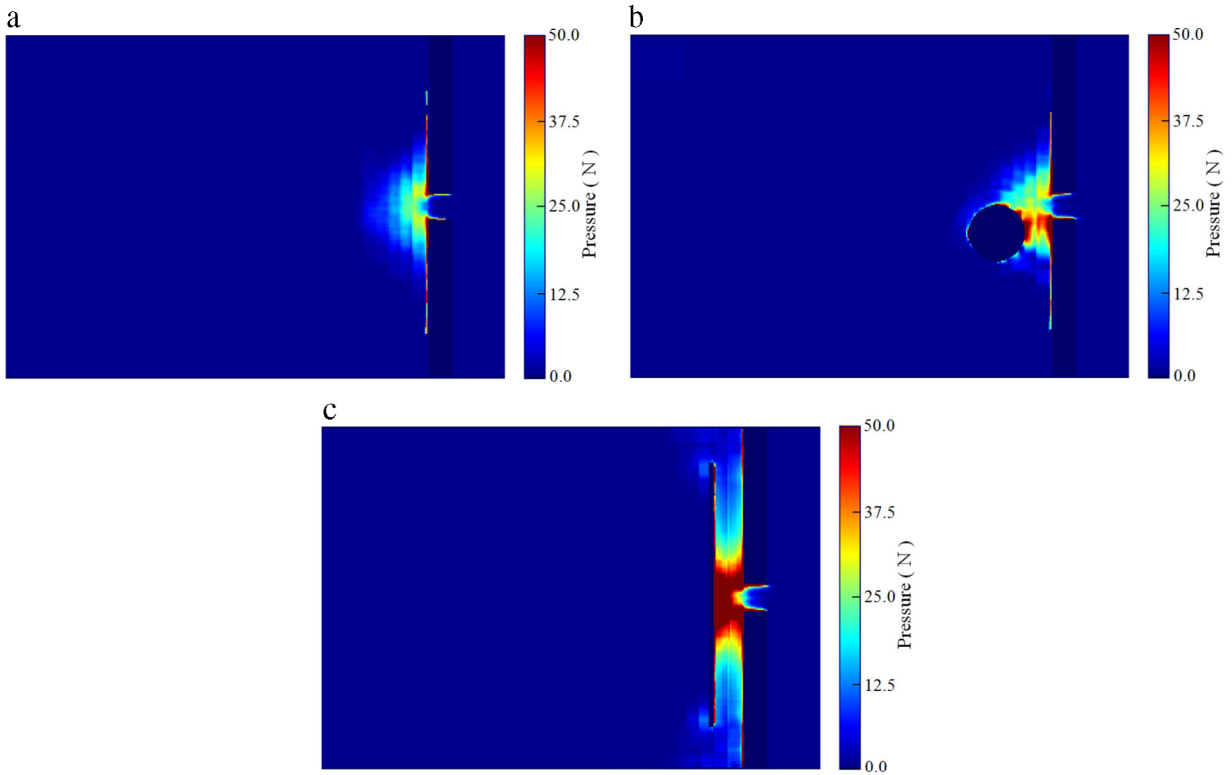


Fig. 13. The spatial distributions of pedestrian pressures for (a) no obstacle, (b) pillar-like obstacle and (c) panel-like obstacle. (For interpretation of the references to color in this figure legend, the reader is referred to the web version of this article.)

center of the channel undergo a higher body pressure force from other people at two sides of the panel which causes the severe body compression of pedestrians in a relative enclosed channel region.

Moreover, to quantitatively compare the pedestrian pressures among no obstacle, pillar-like obstacle and panel-like obstacle, the maximum pressure and the average pressure are further calculated based on the spatial distributions of pedestrian pressures. The original maximum pressure of 138.55 N and average pressure of 2.3 N for no obstacle have been increased to 161.65 N and 3.53 N for pillar-like obstacle, and further promoted to 172.41 N and 6.93 N respectively for panel-like obstacle. Therefore, it is clearly demonstrated that the maximum and average pedestrian pressures in the region of exit are not decreased but surprisingly increased when placing a pillar-like or panel-like obstacle in front of the exit which is markedly different from the hypothesis of existing literature [23,25,26] that placing an obstacle in panic situations might reduce or absorb the pressure in the region of exit.

Although the maximum pressure in the evacuation crowd is getting bigger and bigger, and rises from original 138.55 N–161.65 N and 172.41 N respectively for pillar-like obstacle and panel-like obstacle, the maximum pressure in the crowd does not exceed the maximum endurable force of 242 N for a middle aged male (74 kg) [30,37]. That means, with the pedestrian desired velocity of $v_0 = 1.48$ m/s which refers to our previous literature for escape panics of classroom evacuation in the real-life 2013 Ya'an earthquake in China [30], the enhanced maximum crowd pressure of 161.65 N and 172.41 N for pillar-like obstacle and panel-like obstacle respectively are still safe enough which will not cause heavy injuries in the evacuation crowd.

To sum up, we have proven, with the aid of social force model simulation, that placing an obstacle in panic situations does not reduce or absorb the pressure in the region of exit, on the contrary, promotes the pressure to a much higher level. Therefore, the physical mechanism behind the evacuation performance enhancement while placing an obstacle is not a pressure decrease in the region of exit, but a significant reduction of high density region by effective separation in space which finally causes the increasing of escape speed and evacuation outflow.

6. Robustness verification of evacuation performance

To further verify the robustness and universality of evacuation performance for different shaped obstacles, we have compared the evacuation time among no obstacle, pillar-like obstacle and panel-like obstacle under different initial pedestrian distributions, different initial crowd density, and different desired velocities of escape in this section.

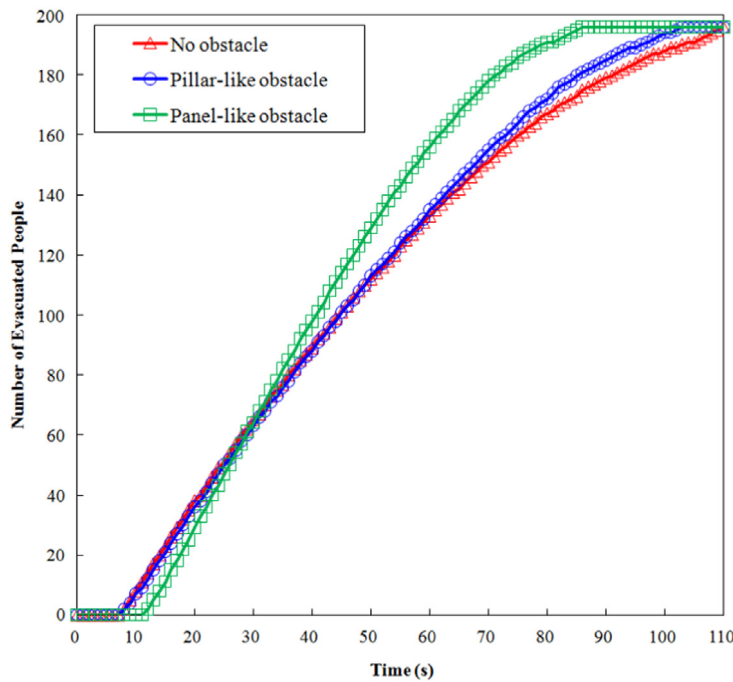


Fig. 14. The evacuated people comparison among no obstacle, pillar-like obstacle and panel-like obstacle respectively at different evacuation time under random initial pedestrian distribution.

6.1. Different initial pedestrian distributions

In the above discussion, the initial pedestrians are all placed in a homogeneously distributed arrangement throughout the $15\text{ m} \times 15\text{ m}$ indoor room. In order to investigate the effect of initial distribution of pedestrian's position on evacuation performance of obstacle, we compare the evacuation time of pedestrians among no obstacle, pillar-like obstacle and panel-like obstacle under random initial pedestrian distribution as shown in Fig. 14. In this study, the average pedestrian evacuation time is calculated based on the evacuation results of 20 escape runs for no obstacle, pillar-like obstacle and panel-like obstacle configuration.

Fig. 14 clearly demonstrates that the initial distribution of pedestrian's position has no obvious influence upon the evacuation performance of obstacle, and the evacuated people number of panel-like obstacle at different evacuation time is still remarkably superior to that of pillar-like obstacle and no obstacle under random initial pedestrian distribution. The evacuation speed curve of pillar-like obstacle is basically consistent with that of no obstacle before the evacuation time of $t = 60\text{ s}$. However, the evacuation efficiency of pillar-like obstacle begins to exceed that of no obstacle after the evacuation time of $t = 60\text{ s}$. Moreover, compared to the uniform initial distribution, the random initial distribution will need more time to evacuate all the people in the room which increases from original 101.1 s , 92.39 s and 77.95 s – 110 s , 103 s and 86 s respectively for no obstacle, pillar-like obstacle and panel-like obstacle because of the randomness and irregularity characteristics of pedestrian initial distribution. On the whole, the influence of different initial pedestrian distributions on evacuation efficiency of obstacle is statistically slight or not obvious in this work because different initial pedestrian distributions could only change the evacuation behaviors of pedestrians in the left initial region, and the overall evacuation behaviors of people in the region of exit remain unchanged for pillar-like obstacle and panel-like obstacle.

6.2. Different initial crowd density

In the above analysis, the total number of evacuated pedestrians is fixed to 196, and the pedestrians are initially placed in a uniform distribution throughout the $15\text{ m} \times 15\text{ m}$ area with an initial crowd density of 0.87 m^{-2} which does not exceed healthy indoor environmental regulations [29]. To investigate the effect of initial crowd density on evacuation performance of obstacle, we compare the evacuation time of pedestrians among no obstacle, pillar-like obstacle and panel-like obstacle under a lower initial crowd density of 0.44 m^{-2} with 100 evacuated pedestrians and a higher initial crowd density of 1.78 m^{-2} with 400 evacuated pedestrians as shown in Fig. 15(a) and (b) respectively.

From the comparison results of Fig. 15(a) and (b), it is obviously seen that the different initial crowd density could markedly influence the evacuation performance of obstacle, and the evacuation efficiency of panel-like obstacle is still superior to that of pillar-like obstacle and no obstacle under different initial crowd density. For the lower initial crowd density of 0.44 m^{-2} in Fig. 15(a), the evacuation efficiency of 100 pedestrians both achieves remarkable improvement for

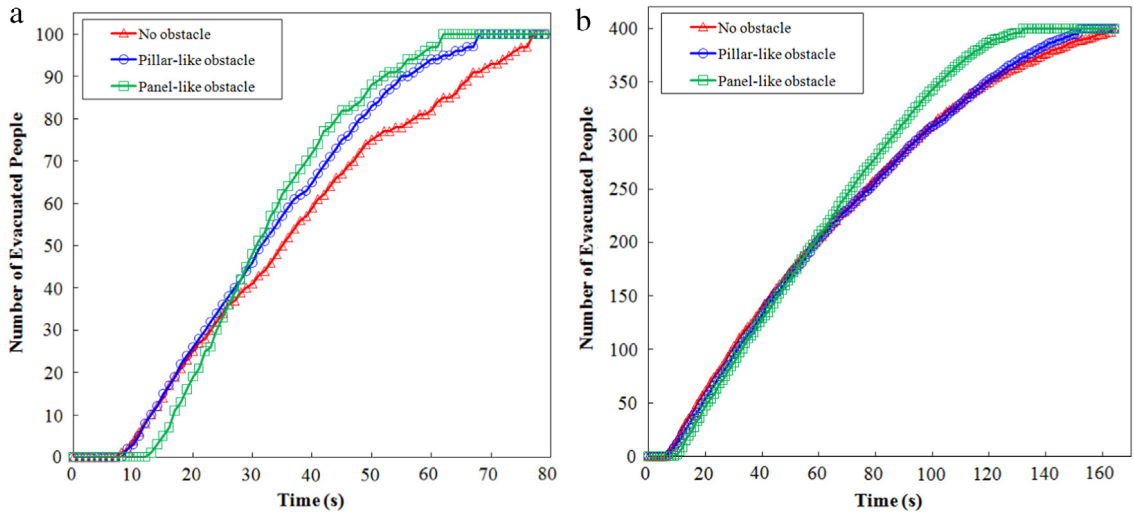


Fig. 15. The evacuated people comparison among no obstacle, pillar-like obstacle and panel-like obstacle respectively at different evacuation time under (a) a lower initial crowd density of 0.44 m^{-2} with 100 evacuated pedestrians and (b) a higher initial crowd density of 1.78 m^{-2} with 400 evacuated pedestrians.

pillar-like obstacle and panel-like obstacle, and the number of evacuated people both exceeds that of no obstacle after the evacuation time of $t = 27 \text{ s}$. The original leaving time of 77 s for the 100 pedestrians has been reduced to 68 s and 62 s respectively when suitably placing a pillar-like obstacle and a panel-like obstacle in front of the exit.

For the higher initial crowd density of 1.78 m^{-2} in Fig. 15(b), the evacuation efficiency of 400 pedestrians obtains significant improvement only for panel-like obstacle, and the number of evacuated people starts to outnumber that of no obstacle after the evacuation time of $t = 65 \text{ s}$. However, the enhancement of evacuation performance for pillar-like obstacle is not obvious because the evacuation speed curve of pillar-like obstacle broadly coincides with that of no obstacle before the evacuation time of $t = 120 \text{ s}$, and its evacuation efficiency obtains slight improvement only after the evacuation time of $t = 120 \text{ s}$. On the whole, the original leaving time of 164 s for the 400 pedestrians has been reduced to 152 s and 132 s respectively when suitably placing a pillar-like obstacle and a panel-like obstacle.

Therefore, the evacuation performance of panel-like obstacle is relatively stable, and not sensitive to the initial crowd density. The evacuation efficiency of pedestrians can achieve remarkable enhancement for both lower and higher initial crowd density when placing a panel obstacle with optimal layout in front of the exit. Relatively speaking, the evacuation performance of pillar-like obstacle severely depends on the initial crowd density. That is to say, the pillar-like obstacle can only promote the evacuation efficiency of pedestrians significantly under a lower initial crowd density because it would be quite difficult for pillar-like obstacle to further effectively reduce the high density region of exit by separation in space in an already overcrowded room with a higher initial crowd density.

6.3. Different desired velocities of escape

The desired velocity of pedestrians is all set to $v_0 = 1.48 \text{ m/s}$ in the above discussions which refers to our previous literature for escape panics of classroom evacuation where the people were all evacuated from the classroom orderly under the guidance of the teacher when the earthquake occurred [30]. However, to further verify the robustness and universality of evacuation performance for different shaped obstacles, we have also compared the evacuation time among no obstacle, pillar-like obstacle and panel-like obstacle under a desired velocity of $v_0 = 1.0 \text{ m/s}$ for the normal situation and $v_0 = 5.0 \text{ m/s}$ [1] for the disorderly panic evacuation situation as shown in Fig. 16(a) and (b) respectively.

Fig. 16 clearly demonstrates that the evacuation efficiency enhancement of panel-like obstacle is more remarkable and stable than that of pillar-like obstacle under different desired velocities of $v_0 = 1.0 \text{ m/s}$ and 5.0 m/s . For the normal situation of $v_0 = 1.0 \text{ m/s}$ in Fig. 16(a), the total number of evacuated people of panel-like obstacle obviously exceeds that of no obstacle after the evacuation time of $t = 50 \text{ s}$. However, the evacuation speed curve of pillar-like obstacle basically coincides with that of no obstacle during the whole evacuation process except for the middle evacuation stage. The original evacuation time of 165 s for 196 pedestrians has been slightly reduced to 162 s when placing a pillar-like obstacle, and further dramatically decreased to 137 s when placing a panel-like obstacle.

For the panic evacuation situation of $v_0 = 5.0 \text{ m/s}$ in Fig. 16(b), the total number of evacuated people of panel-like obstacle is smaller than that of no obstacle before the evacuation time of $t = 14 \text{ s}$ because the people need to run a relatively longer distance to bypass the panel obstacle to reach the door. After the evacuation time of $t = 14 \text{ s}$, the number of evacuated people of panel obstacle begins to remarkably exceed that of no obstacle and the original evacuation time of 27 s for 196 pedestrians has been decreased to 23 s. However, the evacuation speed curve of pillar-like obstacle almost

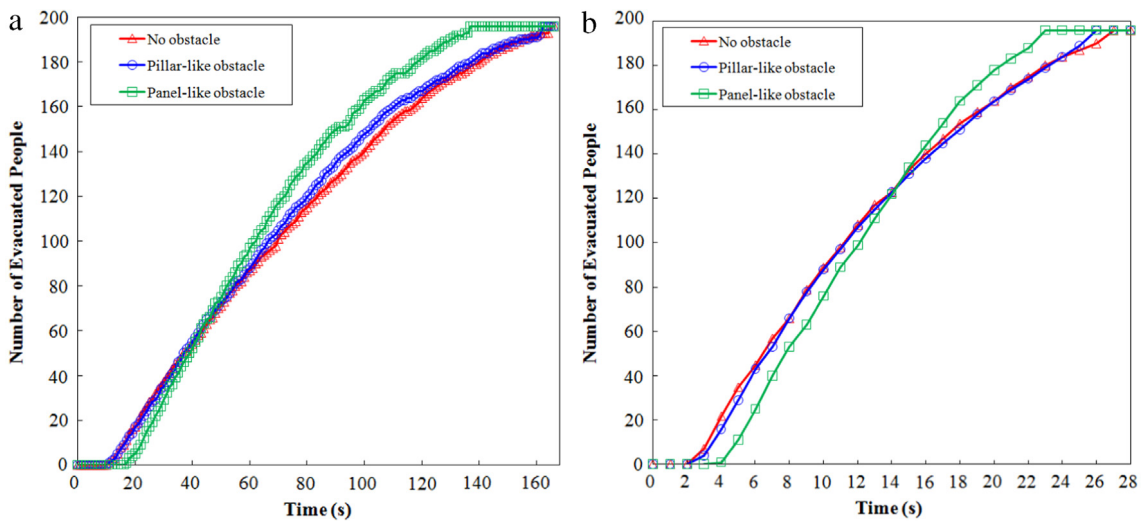


Fig. 16. The evacuated people comparison among no obstacle, pillar-like obstacle and panel-like obstacle at different evacuation time under a desired velocity of (a) $v_0 = 1.0$ m/s and (b) $v_0 = 5.0$ m/s respectively.

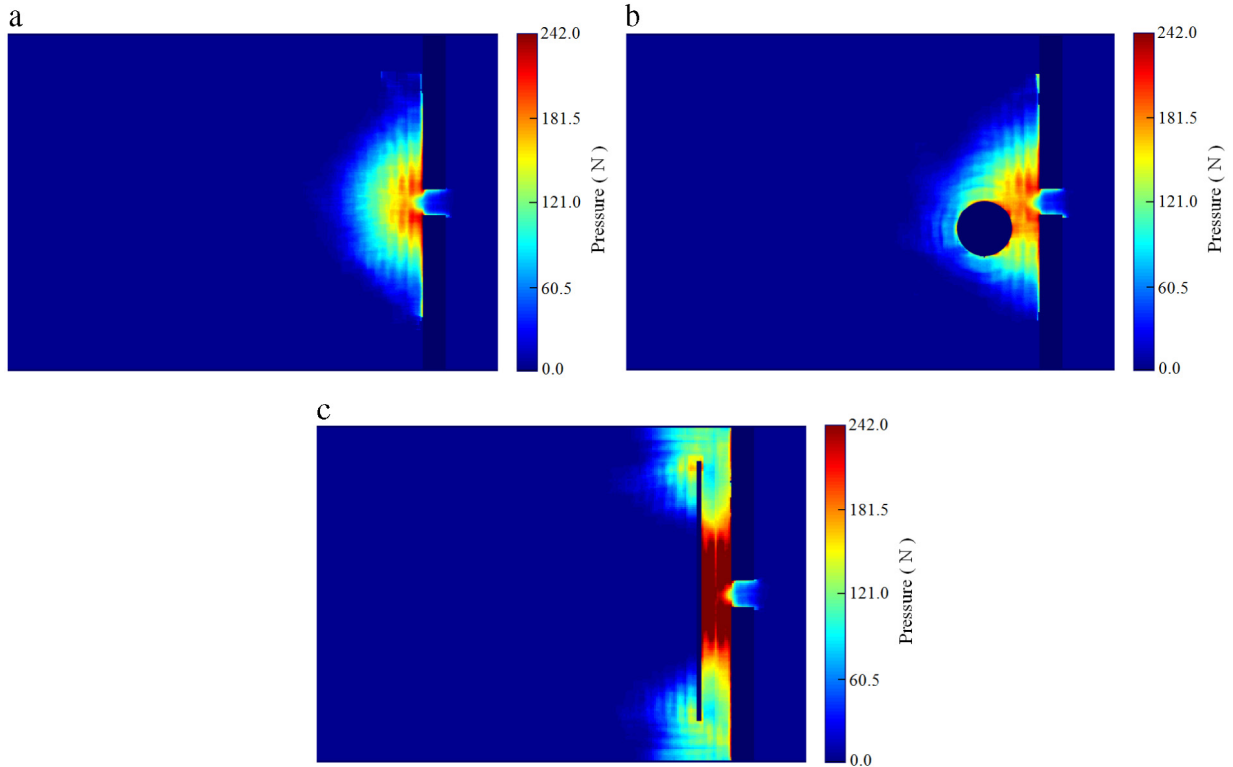


Fig. 17. The spatial distributions of pedestrian pressures for (a) no obstacle, (b) pillar-like obstacle and (c) panel-like obstacle under the desired velocity of $v_0 = 5.0$ m/s. (For interpretation of the references to color in this figure legend, the reader is referred to the web version of this article.)

completely coincides with that of no obstacle during the whole evacuation process, and the original evacuation time of 27 s has been slightly reduced to 26 s which means the evacuation efficiency enhancement of pillar-like obstacle is statistically negligible or not obvious for the panic evacuation situation of $v_0 = 5.0$ m/s.

Finally, to further investigate the effect of high desired velocities on pedestrian pressures, we compare the spatial distributions of pedestrian pressures for no obstacle, pillar-like obstacle and panel-like obstacle under the desired velocity of $v_0 = 5.0$ m/s as shown in Fig. 17(a)–(c) respectively. In Fig. 17, it is clearly demonstrated that the high pressure area of above 242 N (dark red area) is getting bigger and bigger for no obstacle, pillar-like obstacle and panel-like obstacle.

In Fig. 17(a), the high pressure areas of above 242 N with dark red color mainly appears around exit zone. In Fig. 17(b), the high pressure area of above 242 N is concentrated at the region between the pillar and the wall in front owing to the body conflicts in this relative enclosed space. In Fig. 17(c), a big high pressure area of above 242 N with dark red color is located at the center of the channel between the panel and the wall in front because of the high body force from other people at two sides of the panel which causes the severe body compression of pedestrians in an enclosed channel region. The average pressure in the evacuation crowd is getting higher and higher which rises from original 9.84 N to 11.03 N and 19.39 N respectively for pillar-like and panel-like obstacle. Because the maximum endurable force for a middle aged male (74 kg) is 242 N [30,37], the maximum pressure of 344.81 N for no obstacle have been further promoted to a more dangerous level of 362.32 N and 473.51 N respectively for pillar-like obstacle and panel-like obstacle.

Therefore, under the panic evacuation situation of $v_0 = 5.0$ m/s, placing an obstacle in front of the exit will promote the crowd pressure to a more dangerous level, especially for panel-like obstacle, which could cause more serious injuries in the evacuation crowd. That is to say, when placing a pillar-like or panel-like obstacle with optimal layout in front of the exit to enhance the evacuation efficiency of pedestrians, we should also try to maintain the calm and order of crowd, and decrease the desired velocity of crowd to a much safer level in order to avoid fatal accident to the most degree.

7. Conclusion and future research

The main motivation of this study is to find an optimal layout of obstacles for panic evacuation by using a novel differential evolution technique, and uncover the physical mechanism behind the evacuation efficiency enhancement of obstacles by analyzing the profiles of density, velocity and specific flow, as well as the spatial distribution of crowd pressure.

Firstly, a robust differential evolution (DE) is employed to optimize the geometrical parameters of pillar-like and panel-like obstacles in order to achieve an optimal leaving time for all the pedestrians in the room. It is demonstrated that with the optimal geometrical parameters optimized by differential evolution algorithm, the leaving time of 101.1 s for all the pedestrians has been reduced to 92.39 s and 77.95 s respectively when suitably placing a pillar-like obstacle and a panel-like obstacle in front of the exit. Therefore, the geometrical parameters optimization methodology presented in this paper that uses a social force model optimized by differential evolution technique is a very convenient and efficient way to pursue an optimal obstacle layout in order to obtain a maximum enhancement of evacuation performance.

Secondly, the effects of geometrical parameters of obstacles on evacuation time have also been further analyzed. It is found that the evacuation performances of obstacles are quite sensitive to these geometrical parameters, and the best way for achieving an optimal pedestrian outflow is to slightly shift the obstacle from the center of the exit which is consistent with findings of extant literature. Especially, the effective geometrical parameter ranges of pillar-like obstacle are quite narrow and limited to enhance the evacuation performance, while the effective parameter ranges of panel-like obstacle are relatively broad. That is to say, the panel-like obstacle is actually more robust and stable than the pillar-like obstacle which can guarantee the enhancement of evacuation performance.

Thirdly, in order to uncover the essence of evacuation performance enhancement, the profiles of density, velocity and specific flow for no obstacle, pillar-like obstacle and panel-like obstacle are compared in detail based on the Voronoi method. It is clearly demonstrated that the physical mechanism behind the evacuation performance enhancement while placing an obstacle is a direct decrease of high density region by effective separation in space which will cause the increase in escape speed and evacuation outflow. In this study, the average outflow of outdoor area has been improved by 3.70% and 29.63% respectively when placing a pillar-like and panel-like obstacle with optimal layout in front of the exit. Therefore, compared to the pillar-like obstacle, the panel-like obstacle can more significantly decrease the high density region by effective separation in space, and increase the escape speed of pedestrians near the area of exit which finally leads to the more remarkable enhancement of pedestrian outflow.

Fourthly, to further investigate whether placing an obstacle can reduce the pressure in the region of exit or, on the contrary, increase the pressure to a more dangerous level, the maximum pressure, the average pressure, and the spatial distribution of pedestrian pressures among no obstacle, pillar-like obstacle and panel-like obstacle are analyzed. The original maximum crowd pressure of 138.55 N and average pressure of 2.3 N for no obstacle have been increased to 161.65 N and 3.53 N for pillar-like obstacle, and further promoted to 172.41 N and 6.93 N respectively for panel-like obstacle. That means the maximum and average crowd pressures in the region of exit are not decreased but surprisingly increased when placing a pillar-like or panel-like obstacle in front of the exit which is markedly different from the hypothesis of existing literature that placing an obstacle in panic situations might reduce or absorb the pressure in the region of exit.

Finally, to further verify the robustness and universality of evacuation performance for different shaped obstacles, we have also compared the evacuation time under different initial pedestrian distributions, different initial crowd density, and different desired velocities of escape. It is demonstrated that the influence of different initial pedestrian distributions on evacuation efficiency of obstacle is statistically slight or not obvious because different initial pedestrian distributions could only change the evacuation behaviors of pedestrians in the left initial region, and the overall evacuation behaviors of people in the region of exit remain unchanged. Moreover, the evacuation performance of panel-like obstacle is relatively stable, and not sensitive to the initial crowd density, while the performance of pillar-like obstacle severely depends upon the initial crowd density. That means the pillar-like obstacle can only improve the evacuation efficiency significantly under a lower initial crowd density because it would be quite hard for pillar-like obstacle to further reduce the high density region of exit by separation in space in an already overcrowded room with a higher initial crowd density. Similarly, the evacuation efficiency

enhancement of panel-like obstacle is more significant and stable under different desired velocities of $v_0 = 1.0$ and 5.0 m/s, however, the enhancement of pillar-like obstacle is statistically negligible or not obvious for the panic evacuation situation of $v_0 = 5.0$ m/s. Especially, under the panic evacuation situation of $v_0 = 5.0$ m/s, placing an obstacle in front of the exit will promote the crowd pressure to a more dangerous level, hence we should try to control the desired velocity of crowd to a much safer level in order to avoid serious injuries in the evacuation crowd.

To sum up, we have proven, with the aid of numerical modeling, that placing an obstacle in panic situations does not reduce or absorb the pressure in the region of exit, on the contrary, promotes the pressure to a much higher level, and the physical mechanism behind the evacuation performance enhancement while placing an obstacle is not a pressure decrease in the region of exit, but a significant reduction of high density region by effective separation in space which finally causes the increasing of escape speed and evacuation outflow. Moreover, the panel-like obstacle is considerably more robust and stable than the pillar-like obstacle to guarantee the enhancement of evacuation efficiency under different initial pedestrian distributions, different initial crowd densities as well as different desired velocities.

In the future, we will try to perform a series of human experiments to confirm that the panel-like obstacle is more robust and stable than the pillar-like obstacle to guarantee the enhancement of evacuation efficiency. Moreover, in the simulated and human experiments, the layout design of pillar-like obstacle with one pillar and two pillars should be further compared to validate that two pillar-like obstacles are better than one pillar-like obstacle.

Furthermore, in real-life evacuation scenes of fire, flooding or tsunami, the parameter values of proposed social force model in this paper could be substantially different and varying individually because of different building environments, disaster characteristics, panic behaviors and guiding strategies. That means the proposed social force model itself should be further extended according to different disaster characteristics, such as developing a 3D social force model for evacuation scene on stairs and should also be calibrated and validated by all kinds of trajectory extracting techniques, such as video tracking technology or UWB-based indoor positioning system.

Acknowledgments

This work is supported by National Natural Science Foundation of China (Grant Nos. 71303051, 71203028, 71522014, 71301028, 61300103), MOE (Ministry of Education in China) Project of Humanities and Social Sciences (Grant No. 13YJCZH270), Major Project Funding for Social Science Research Base in Fujian Province Social Science Planning (No. FJ2015JDZ030), China Scholarship Council (Grant Nos. 201406655011, 201506655018), Program for Distinguished Young Research Talents in Higher Education Institutions of Fujian Province, China (Grant No. JA13043S) and Logistics Research Center of Fuzhou University, Fujian Social Sciences Research Base.

References

- [1] D. Helbing, I. Farkas, T. Vicsek, Simulating dynamical features of escape panic, *Nature* 407 (2000) 487–490.
- [2] D. Helbing, I. Farkas, T. Vicsek, Freezing by heating in a driven mesoscopic system, *Phys. Rev. Lett.* 84 (2000) 1240–1243.
- [3] D. Helbing, P. Molnar, Social force model for pedestrian dynamics, *Phys. Rev. E* 51 (1995) 4282–4286.
- [4] C. Burstedde, K. Klauck, A. Schadschneider, J. Zittartz, Simulation of pedestrian dynamics using a two-dimensional cellular automaton, *Physica A* 295 (2001) 507–525.
- [5] A. Kirchner, A. Schadschneider, Simulation of evacuation processes using a bionics-inspired cellular automaton model for pedestrian dynamics, *Physica A* 312 (2002) 260–276.
- [6] A. Kirchner, H. Klüpfel, K. Nishinari, A. Schadschneider, M. Schreckenberg, Simulation of competitive egress behavior: comparison with aircraft evacuation data, *Physica A* 324 (2003) 689–697.
- [7] M. Muramatsu, T. Nagatani, Jamming transition in two-dimensional pedestrian traffic, *Physica A* 275 (2000) 281–291.
- [8] Y. Tajima, T. Nagatani, Clogging transition of pedestrian flow in T-shaped channel, *Physica A* 303 (2002) 239–250.
- [9] S. Manica, Traffic jamming on hexagonal lattice, *Physica A* 321 (2003) 653–664.
- [10] D. Helbing, M. Isobe, T. Nagatani, K. Takimoto, Lattice gas simulation of experimentally studied evacuation dynamics, *Phys. Rev. E* 67 (2003) 067101.
- [11] J. MacGregor Smith, F.R.B. Cruz, M/G/c/c state dependent travel time models and properties, *Physica A* 395 (2014) 560–579.
- [12] D.L. Zhao, J. Li, Y. Zhu, L. Zou, The application of a two-dimensional cellular automata random model to the performance-based design of building exit, *Build. Environ.* 43 (2008) 518–522.
- [13] W.K. Chow, C.M.Y. Ng, Waiting time in emergency evacuation of crowded public transport terminals, *Saf. Sci.* 46 (2008) 844–857.
- [14] A. Seyfried, O. Passon, B. Steffen, M. Boltes, T. Rupprecht, W. Klingsch, New insights into pedestrian flow through bottlenecks, *Transp. Sci.* 43 (2009) 395–406.
- [15] X. Xu, W.G. Song, Staircase evacuation modeling and its comparison with an egress drill, *Build. Environ.* 44 (2009) 1039–1046.
- [16] H. Weckman, S. Lehtimaki, S. Mannikko, Evacuation of a theatre: Exercise vs calculations, *Fire Mater.* 23 (1999) 357–361.
- [17] S.T. Rassia, C.I. Siettos, Escape dynamics in office buildings: Using molecular dynamics to quantify the impact of certain aspects of human behavior during emergency evacuation, *Environ. Model. Assess.* 15 (2010) 411–418.
- [18] G. Lämmel, D. Grether, K. Nagel, The representation and implementation of time-dependent inundation in large-scale microscopic evacuation simulations, *Transp. Res. C* 18 (2010) 84–98.
- [19] G. Frank, C. Dorso, Room evacuation in the presence of an obstacle, *Physica A* 390 (2011) 2135–2145.
- [20] L. Jiang, J. Li, C. Shen, S. Yang, Z. Han, Obstacle optimization for panic flow - reducing the tangential momentum increases the escape speed, *PLoS One* 9 (2014) e115463.
- [21] A. Johansson, D. Helbing, Pedestrian flow optimization with a genetic algorithm based on boolean grids, in: *Pedestrian and Evacuation Dynamics 2005*, Springer, Berlin, Heidelberg, 2006, pp. 267–272.
- [22] D. Yanagisawa, R. Nishi, A. Tomoeda, K. Ohtsuka, A. Kimura, et al., Study on efficiency of evacuation with an obstacle on hexagonal cell space, *SICE J. Control Meas. Syst. Integr.* 3 (2010) 395–401.
- [23] Z. Iker, J. Alvaro, G. Angel, et al., Silo clogging reduction by the presence of an obstacle, *Phys. Rev. Lett.* 107 (2011) 278001.
- [24] F. Alonso-Marroquin, S.I. Azeezullah, S.A. Galindo-Torres, L.M. Olsen-Kettle, Bottlenecks in granular flow: when does an obstacle increase the flow rate in an hourglass? *Phys. Rev. E* 85 (2012) 020301.

- [25] D. Helbing, L. Buzna, A. Johansson, T. Werner, Self-organized pedestrian crowd dynamics: experiments, simulations, and design solutions, *Transp. Sci.* 39 (2005) 1–24.
- [26] A. Kirchner, K. Nishinari, A. Schadschneider, Friction effects and clogging in a cellular automaton model for pedestrian dynamics, *Phys. Rev. E* 67 (2003) 056122.
- [27] D. Yanagisawa, A. Kimura, A. Tomoeda, R. Nishi, Y. Suma, K. Ohtsuka, K. Nishinari, Introduction of frictional and turning function for pedestrian outflow with an obstacle, *Phys. Rev. E* 80 (2009) 036110.
- [28] D. Parisi, C. Dorso, Microscopic dynamics of pedestrian evacuation, *Physica A* 354 (2005) 606–618.
- [29] M. MySEN, S. Berntsen, P. Nafstad, P. Schild, Occupancy density and benefits of demand-controlled ventilation in norwegian primary schools, *Energy Build.* 37 (2005) 1234–1240.
- [30] M. Li, Y. Zhao, L. He, W. Chen, X. Xu, The parameter calibration and optimization of social force model for the real-life 2013 Ya'an earthquake evacuation in China, *Saf. Sci.* 79 (2015) 243–253.
- [31] A. Johansson, D. Helbing, P.K. Shukla, Specification of the social force pedestrian model by evolutionary adjustment to video tracking data, *Adv. Complex Syst.* 10 (2007) 271–288.
- [32] Y.X. Zhao, F. Chen, Q. Shen, L.M. Zhang, Optimal design of graded refractive index profile for broadband omnidirectional antireflection coatings using genetic programming, *Prog. Electromagn. Res.* 145 (2014) 39–48.
- [33] R. Storn, K. Price, Differential evolution—a simple and efficient heuristic for global optimization over continuous spaces, *J. Global Optim.* 11 (1997) 341–359.
- [34] Y.X. Zhao, F. Chen, Q. Shen, Q.W. Liu, L.M. Zhang, Optimizing low loss negative index metamaterial for visible spectrum using differential evolution, *Opt. Express* 19 (2011) 11605–11614.
- [35] J. Zhang, W. Klingsch, A. Schadschneider, A. Seyfried, Transitions in pedestrian fundamental diagrams of straight corridors and T-junctions, *J. Stat. Mech. Theory Exp.* 2011 (2011) P06004.
- [36] B. Steffen, A. Seyfried, Methods for measuring pedestrian density, flow, speed and direction with minimal scatter, *Physica A* 389 (2010) 1902–1910.
- [37] L. Paul, M. Robert, N.A. Basel, Crowd dynamics discrete element multi-circle model, *Saf. Sci.* 44 (2006) 395–417.